

AFCRL-66-49

TRANSVERSE ANTENNA FEEDS

By David F. Bowman

RADIO CORPORATION OF AMERICA
MISSILE AND SURFACE RADAR DIVISION
MOORESTOWN, NEW JERSEY

Contract No. AF 19(628)-2758
Project No. 4600
Task No. 46007

FINAL REPORT

Period Covered: January 1963 to December 1965
January 1966

Prepared for

AIR FORCE CAMBRIDGE RESEARCH LABORATORIES
OFFICE OF AEROSPACE RESEARCH
UNITED STATES AIR FORCE
BEDFORD, MASSACHUSETTS

CLEARING FEE FOR FUNDAMENTAL SCIENCE TECHNICAL INFORMATION		
Hardcopy Microfilm		
\$7.60	\$0.75	71 as
A FIVE CENT		

coche /

CRL-66-49

AD 628500

TRANSVERSE ANTENNA FEEDS

By David F. Bowman

RADIO CORPORATION OF AMERICA
MISSILE AND SURFACE RADAR DIVISION
MOORESTOWN, NEW JERSEY

Contract No. AF 19(628)-2758
Project No. 4600
Task No. 46007

FINAL REPORT

Period Covered: January 1963 to December 1965
January 1966

Prepared for

AIR FORCE CAMBRIDGE RESEARCH LABORATORIES
OFFICE OF AEROSPACE RESEARCH
UNITED STATES AIR FORCE
BEDFORD, MASSACHUSETTS

DISTRIBUTION OF THIS
DOCUMENT IS UNLIMITED

ABSTRACT

This study of the transverse focal region of a spherical reflector includes theoretical analyses centered on geometric optics, on vector polarization and on diffraction integrals of physical optics and their evaluation by the method of stationary phase. The results of the numerical evaluation of the focal region field for an incoming wave of uniform amplitude and phase agree with experimental measurements taken on a 10-ft. spherical reflector operating at 24 Gc. An annular step disc feed was designed using the calculated field as a basis. This transverse feed is designed to correct for spherical aberration over an included angle of the sphere of 120 degrees. The measured secondary patterns show agreement with the theory in the region of the main lobe. The disagreement in the area of the side lobes is attributed partly to blockage introduced by the feed horn support and partly to incomplete control of illumination amplitude. Methods are described for minimizing complexity due to polarization and for determining feed distributions required for non-uniform amplitude aperture distributions.

TABLE OF CONTENTS

<u>Section</u>		<u>Page</u>
1	INTRODUCTION	1
2	THEORETICAL DETERMINATION OF FOCAL REGION FIELDS	3
2.1	Review of Geometric Optics	3
2.2	The Three Rays and Their Designation	5
2.3	Simplified Description of Focal Region Field	8
2.4	Equivalence Between Patterns and Distributions in a Spherical System	16
2.5	Feed Distributions for Other Than Uniform Aperture Distributions	17
3	EXPERIMENTAL DETERMINATION OF FOCAL REGION FIELDS	20
3.1	Experimental Set-Up	20
3.2	Results of Experimental Measurements	23
4	AN EXPERIMENTAL TRANSVERSE CORRECTING FEED	32
4.1	Selection of Reflection Type Annular Step Disc Feed	32
4.2	Basis of Design of Experimental Feed	34
4.3	Experimental Evaluation of ASDF	37
5	CONCLUSIONS	52
	REFERENCES	57
	CONTRIBUTIONS AND ACKNOWLEDGEMENTS	58
	APPENDIX A - CIRCULAR APERTURE WITH $J_0(vr)$ TAPER	59
	APPENDIX B - A CONCRETE REFLECTOR FOR EXPERIMENTAL WORK	63

LIST OF ILLUSTRATIONS

<u>Figure</u>		<u>Page</u>
1	Spherical Cap and Incident and Reflected Ray	4
2	Geometry of Circular Section	5
3	Caustic by Geometric Ray Tracing	6
4	Path-Length in a Plane	7
5	Tubular Pencil of Rays Typical of Ray 3	10
6	Power Density in the Focal Region Based on Geometric Optics	11
7	Characteristic Dimensions of $L-\theta_p$ Fishtail Curves	13
8	Spherical Reflector at Receiving Terminal with Probe for Sampling Tangential Component of Focal Region Field in Experimental Set Up	21
9	Theoretical and Experimental Focal Region Distribution Taken in Plane of Sampling Dipole for Principal Polarization Component	24
10	Theoretical and Experimental Focal Region Distribution Taken in Plane Perpendicular to Sampling Dipole for Principal Polarization Component	25
11	Theoretical and Experimental Focal Region Distribution in $\phi = 0$ Plane for \hat{k} and Radial Components of Polarization, Respectively	26
12	Theoretical and Experimental Focal Region Distribution in $\phi = 45^\circ$ Plane for Principal Polarization and for Tangential Cross Polarization Components	28
13	Theoretical and Experimental Focal Region Distribution in $\phi = 45^\circ$ Plane for \hat{k} and Radial Components, Respectively	29
14	Variation of Sidelobe Level	30
15	Variation of Sidelobe Angle	31
16	Annular Step Disc Feeds	33

ILLUSTRATIONS (con't.)

<u>Figure</u>		<u>Page</u>
17	Illumination of Annular Step Mirror	36
18	Phase Design of Experimental Feed	38
19	Cross Section of Annular Step Mirror	39
20	Experimental Annular Step Disc Feed	40
21	Patterns of ASDF, Polarization Perpendicular to Horn Support	42
22	Patterns of ASDF, Polarization in Plane of Horn Support	43
23	Beamwidth as Function of Feed Position, Perpendicular Polarization	44
24	Pattern Level as Function of Feed Position, Perpendicular Polarization	45
25	Beamwidth as Function of Feed Position, Parallel Polarization	46
26	Pattern Level as Function of Feed Position, Parallel Polarization	47

LIST OF TABLES

<u>Table</u>		
1	Summary of Pattern Characteristics of Annular Step Disc Feed	48
2	Pattern Characteristics Averaged by Category	49
3	Comparison to Theoretical Pattern of 140-Wavelength Diameter Uniform Circular Aperture	51

SECTION 1

INTRODUCTION

This report concludes a study for AFCRL on Contract AF 19(628)-2758 "Transverse Antenna Feeds". The purpose of the study is first, to evaluate the electromagnetic field in the focal region of a spherical reflector and second, to design a transverse antenna feed array that will correct for the inherent spherical aberration of the sphere and provide limited beam scanning at microwave frequencies.

The evaluation of the focal-region fields includes theoretical and experimental portions. Previous reports issued on this contract (References 1, 2 and 3) cover in detail the theoretical analysis of the spherical reflector. In Reference 1 are considered useful concepts of geometric optics, namely ray tracing, optical path lengths, description of the focal region, information on the circle of least confusion, and elementary Huygens wave theory. In Reference 2 polarization effects are analyzed by application of the current distribution method in determining the scattered fields. Expressions for the current distribution on the reflector and for the effective current, that radiating in the direction of the circle of least confusion, are derived. Formulas for the fields reflected from the tangent plane are given in terms of direction cosines. In Reference 3 these results are applied in the development of an integral expression for the field in the focal region. The method of stationary phase is applied to the evaluation of this integral. Computed numerical results are given for selected cases of interest in terms of the amplitude and phase of focal-region electric field components parallel to each of three orthogonal axes.

In the work described above emphasis was placed upon the focusing properties of the spherical reflector for a point object at a great distance. The focal region field distributions were computed for this case. The assumption was made, without loss of generality, that the incoming plane wave received by the spherical reflector is linearly polarized in the \hat{z} direction. The range of validity for the calculated focal region field does not include those portions of the focal region at, and near to, the caustic surface or the axial caustic.

One purpose of this report is to cover the experimental evaluation of focal region fields undertaken to confirm the theoretical results of Reference 3 and to extend the knowledge to the regions of the caustics.

This report extends the theoretical analysis by describing an equivalence between focal region distributions and far field patterns. A method is described for transforming the focal region field distribution for a distant point object into a focal region feed distribution resulting in one of many usefully tapered aperture distribution functions.

Another purpose is to describe the development of a transverse feed, the design of which is based on the known distributions of focal region fields, and the experimentally determined performance of this feed in successfully approximating a uniform in-phase aperture distribution when used with a spherical reflector.

SECTION 2

THEORETICAL DETERMINATION OF FOCAL REGION FIELDS

2.1 REVIEW OF GEOMETRIC OPTICS

The sphere is the simplest of all three-dimensional surfaces because its radius of curvature is constant. Consequently, it has no preferential direction and every radius (or normal) passes through its center and is an axis of symmetry. Also, every plane section through the center is a great circle. These properties will now be applied to the optics.

Consider a parallel pencil of rays incident on the concave side of a spherical cap as in Figure 1. The optics is simplified if the incident ray through the center O of the sphere, the central ray, is chosen as the axis. The law of reflection states, (a) that the reflected ray lies in the plane of incidence (the plane containing the normal to the surface, OB and the incident ray AB), and (b) that the angle of reflection equals the angle of incidence. The plane of incidence therefore contains the center, which lies on the normal, as well as the axis, and intersects the sphere in a great circle. It follows that (a) all problems of reflection of a single ray reduce to that of reflection from a circle; and (b) all reflected rays intersect the axis. There can therefore be no skew rays (rays that miss the axis), as there are in the off-axis illumination of the paraboloid. It further follows that all incoming linearly polarized waves are treated alike.

Incoming rays, parallel to and very near the ray passing through the center of the sphere, pass through a focus F called the paraxial focus located half-way down the central ray from the center of curvature to the spherical reflector. In general, for any doubly curved reflector all reflected rays are tangent to two caustic surfaces. A caustic is defined as the envelope of reflected (or refracted) rays as the position of the point of incidence is varied. It is a region of high energy density. All rays incident on the reflector the same distance from the central ray, upon reflection intersect at the same point on this ray. This point moves from the paraxial focus toward the vertex as the incident rays go from the central ray outwards, thus forming a line, the axial caustic, which is a degenerate caustic surface. All reflected rays intersect this line.

Consider now a typical ray AB incident on the spherical reflector at B (see Figure 1). It is parallel to the central ray and separated from it by a distance h . Let the center of the sphere (center of curvature of the reflector) be O, the point of incidence of the central ray on the reflector be V, and the coordinate system have its origin at O and axes as shown. Then h is the length $|OA|$, where A is the foot of the perpendicular from O. Let the angle between the incident ray and the normal, $\angle ABO$, be α . Then by the laws of reflection noted earlier the angle of reflection $\angle OBF_1$ is also α , and

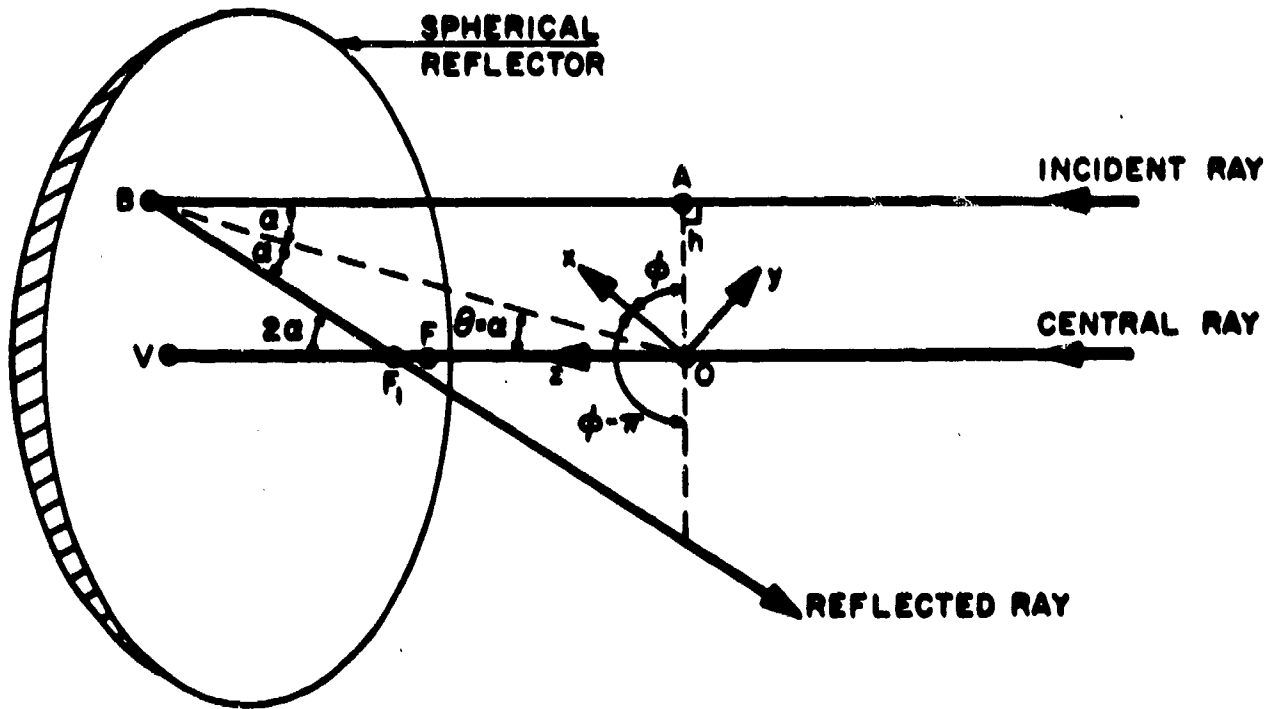


Figure 1. Spherical Cap and Incident and Reflected Ray

further, the reflected ray, the normal and the incident ray all lie in the same plane, i.e., points O , B , A lie in the plane of incidence. But AB is parallel to OV , therefore the plane contains the central ray, and further, the coordinate angle θ of the point B equals α . Thus the reflected ray must intersect OV , say at F_1 . In terms of our coordinate system, since the z axis lies along the central ray, OA lies in the x - y plane, at angle ϕ with respect to the x -axis, and the plane of incidence is characterized by the angles β and $\phi - \pi$. The other two important parameters are h and θ (or α).

There is no loss in generality if we let $\phi = 0$, as in Figure 2. Here again $\theta = \alpha$, and the reflected ray makes an angle 2α with the central ray.

Point C can be shown to be on the caustic surface. A narrow bundle of rays close to AB but in the plane of Figure 2 will focus at C . Figure 3 shows the caustic surface as the envelope of the reflected rays or the locus of C . The caustic surface together with the marginal rays as shown in Figure 4 determine by their intersection line C_1C_1 which is the diameter of "the circle of least confusion", the smallest circle that contains all the rays. The marginal ray may be defined as that striking the rim of the spherical cap

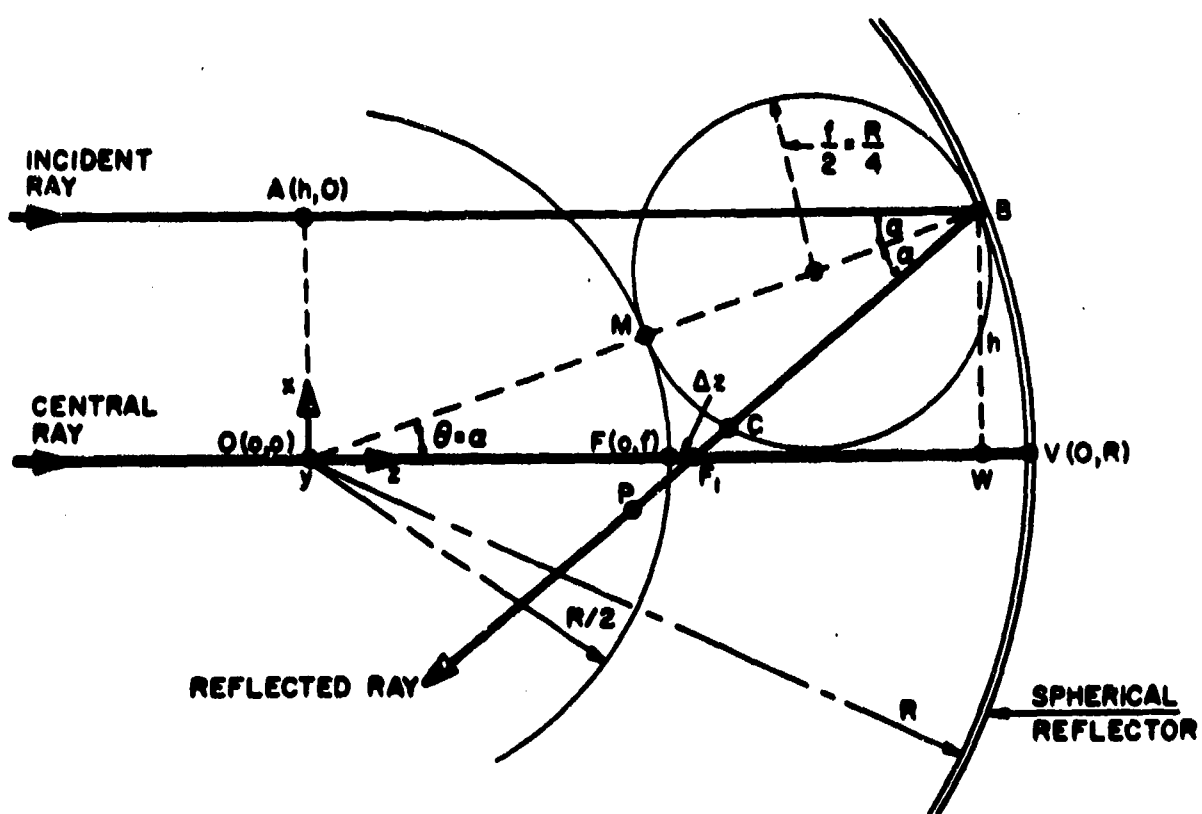


Figure 2. Geometry of Circular Section

reflector as suggested by the figure. More often it is convenient to define the marginal ray by some value h_{\max} or θ_{\max} . In the case of an antenna intended for scanning over a wide angle, for example, the edge of the reflector would normally be beyond the marginal ray except for near end-of-scan limit conditions.

The focal region, which is of great interest for the subject of transverse feeds, lies between the caustic surfaces and between the paraxial focus and the marginal focus.

Many useful geometric relations with respect to the focal region are formulated in Reference 1 and will not be repeated here.

2.2 THE THREE RAYS AND THEIR DESIGNATION

Any field point lying within the focal region but not on a caustic is associated with three incoming rays of geometric optics or three regions of stationary phase. These are illustrated in Figure 3. The usefulness of

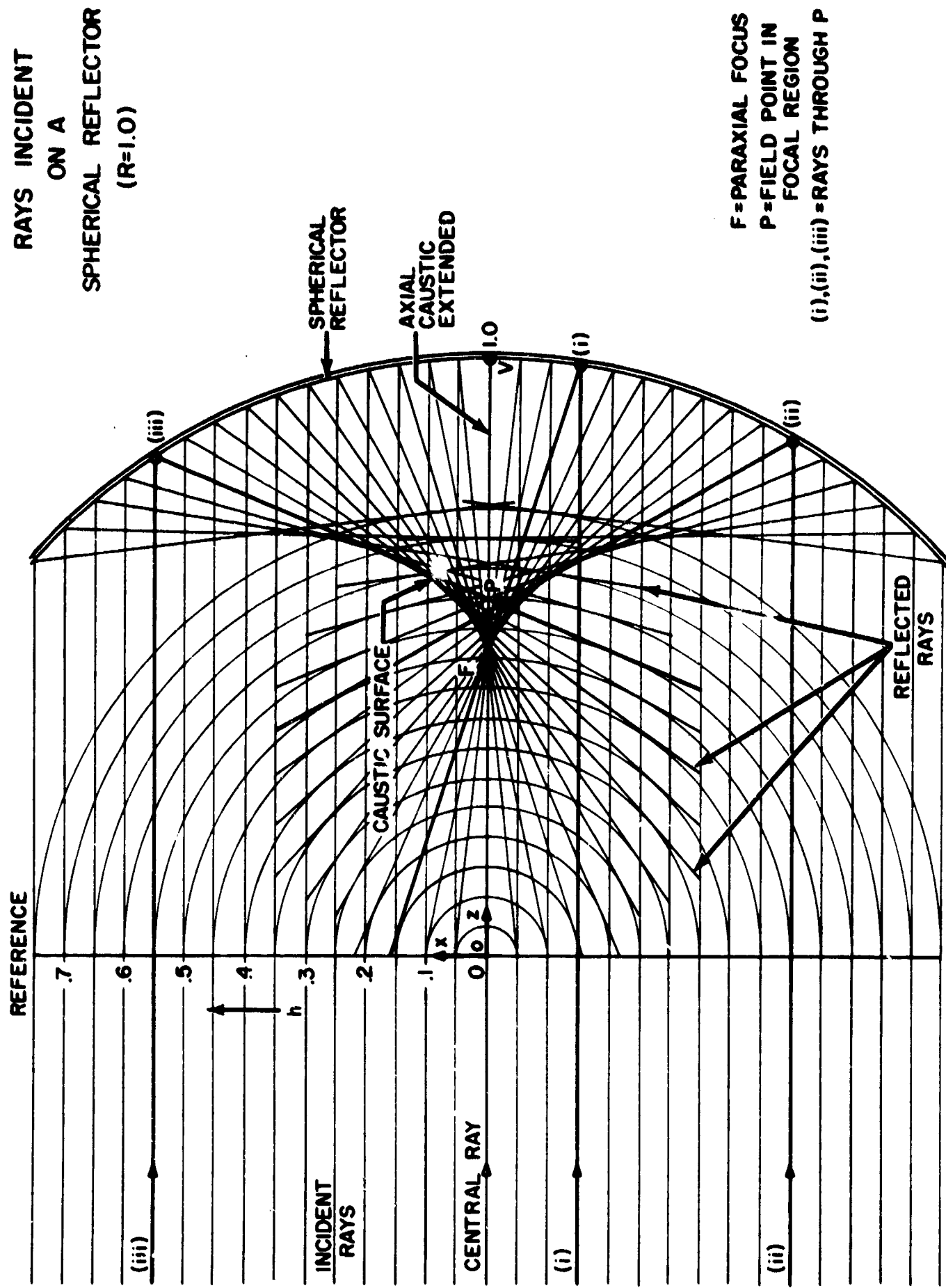


Figure 3. Caustic by Geometric Ray Tracing

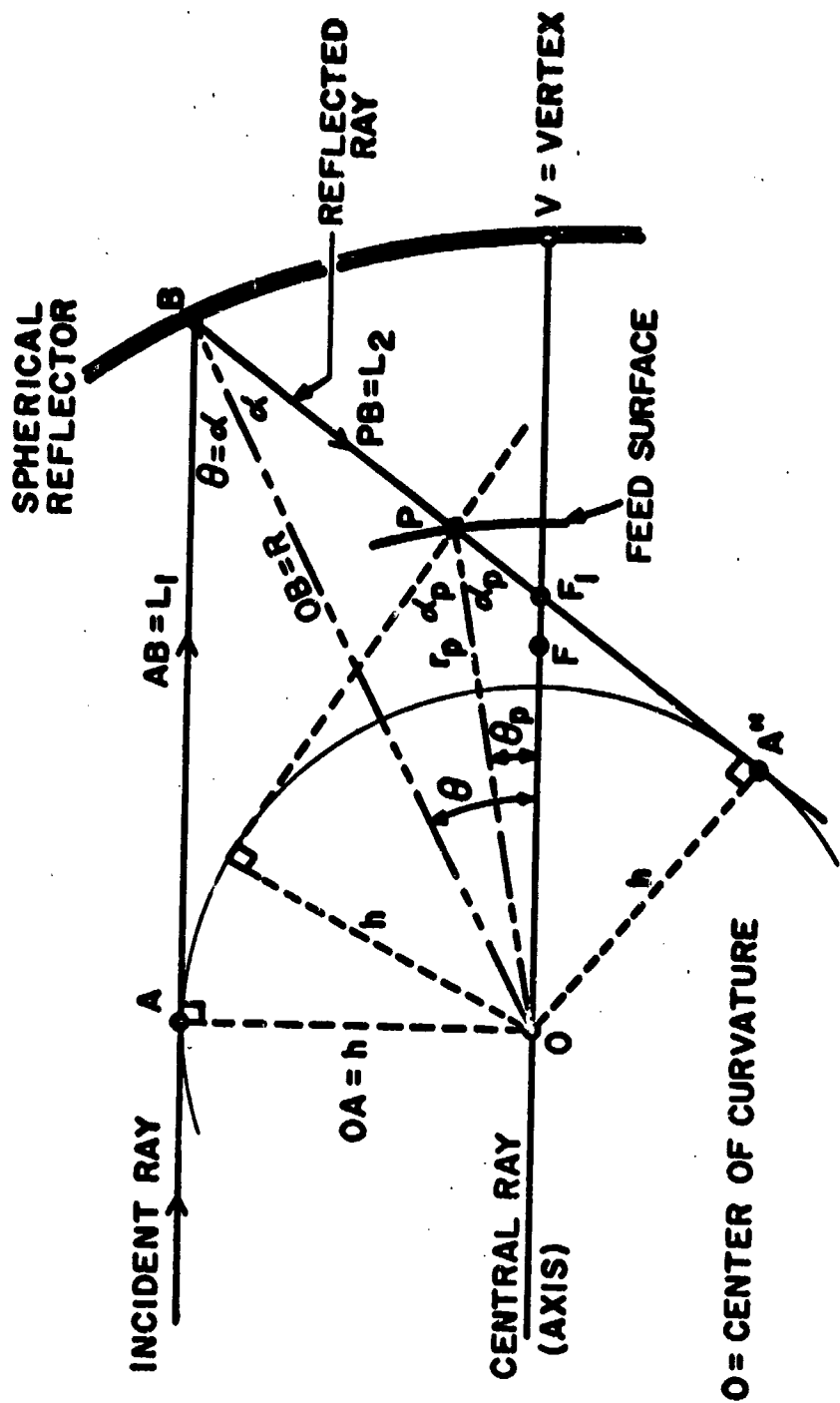


Figure 4. Path-Length in a Plane

describing focal region effects in terms of these three fundamental contributors is apparent.

It is convenient to designate the innermost ray, i.e., the one with smallest value of h or θ and labeled (i) in the figure, as Ray 1, the intermediate ray (ii) as Ray 2 and the outermost ray (iii) as Ray 3. It is to be noted that Rays 1 and 2 always lie on the same side of the axis as the field point, whereas Ray 3 always lies on the side of the axis opposite to that of the field point.

Special cases occur when the field point lies exactly on a caustic. These are still conveniently described by use of similar ray designations although the number of rays is no longer three but is either two or infinity. For example, if the field point lies on the caustic surface, Rays 1 and 2 merge indistinguishably into a single ray while Ray 3 is a separate ray. On the other hand, if the field point lies on the axial caustic, Ray 1 coincides with the axis while Rays 2 and 3 are separate rays but indistinguishable from one another on the basis of h or θ . Moreover, Rays 2 and 3 exist in every plane passing through the axis so the field point coincides with the apex of a cone of an infinite number of rays each inclined at an angle of 2θ with respect to the axis.

The regions of stationary phase follow these same rules inasmuch as the method of stationary phase is being applied to describe the same phenomenon. Thus, in the general case three separate regions (1, 2 and 3) exist. For the field point on the caustic surface only two regions exist. And for the field point on the axial caustic Region 1 is a spot centered about the axis while Regions 2 and 3 merge into a single annular region centered about the axis.

2.3 SIMPLIFIED DESCRIPTION OF FOCAL REGION FIELD

It is useful to consider a simplified description of the focal region field distribution. Great simplification results if the polarization of the wave is neglected. This will be done here. (It will be shown in Section 5.0 that for the case in which the radiating elements of the feed are of a certain class no loss of validity is caused by neglecting polarization effects.) The net field at a generalized field point is composed of contributions from three regions of the reflector surface. In this geometric optics analysis these regions become three points, each corresponding to a ray. Knowledge of the amplitude and phase of the contribution corresponding to each of these rays and variation of the same with respect to field point coordinates is sufficient to estimate the general character of the focal region field distribution.

The amplitude of the contribution can be expressed in terms of the ratio of two cross sectional areas of a pencil of rays, namely, the area at the aperture plane and the area on the spherical feed surface. (The focal regions

in the cases of most interest are spherical-cap circular areas subtending only 5 or 10 degrees in diameter so these may be considered to be plane surfaces for some purposes.) It is convenient to consider the incoming pencil to consist of a hollow tube with a radius h and a wall thickness dh , see Figure 5. The projection of this pencil on the feed sphere with radius r_p is an annulus subtending a half angle θ_p and having a width $d\theta_p$. Power density at the feed surface relative to that at the aperture plane of an incoming wave is the reciprocal of the area ratio or

$$\frac{2\pi h dh}{2\pi r_p \sin\theta_p r_p d\theta_p} = \frac{h}{r_p^2 \sin\theta_p d\theta_p / dh}$$

which may be evaluated readily from computed tables of the component factors.

The graph of Figure 6 shows the variation of this power density for each of the three contributing rays (curves A, B and C) over the focal region for a typical case ($r_p = 0.56$). Curve D represents the sum of the power density values of the three contributions. This is the power distribution if the contributions are combined randomly in phase so it is also the most probable distribution when phase information is lacking or is neglected. Curve E represents the power distribution if the contributions are combined in phase or summed in field. This is a possible (although improbable) condition for restricted values of θ_p .

It is interesting to note that when this set of curves is superimposed upon a similar plot of the corresponding calculated principal-polarization focal-region distribution so that the highest peak of the latter is tangent to the Curve E, then the calculated distribution curve lies above and below the power sum curve, Curve D, for about one half of the total angular extent. (An example is shown later in Figure 17.) In this test case, at least, the designation "most probable" is apparently appropriate for the power sum curve.

A noticeable feature of this graph is the trend toward infinite power densities at the caustics, namely, at θ_p above 2.5 degrees for Rays 1 and 2 and for the sum curve, and at $\theta_p = 0$ for Rays 2 and 3 and for the sum curve. This is a manifestation of the incompleteness of adequacy of the geometric approximation in these areas. Other conditions are also noteworthy. Ray 1 has a finite minimum at the axis. Ray 2 is the strongest ray throughout the focal region and represents approximately half of the total power, that is, Curve B lies about 3 db below Curve D. Rays 1 and 3, though individually weaker than Ray 2, have sufficient combined amplitude throughout the θ_p range that a three-ray vector sum of zero amplitude is possible for certain relative phase conditions.

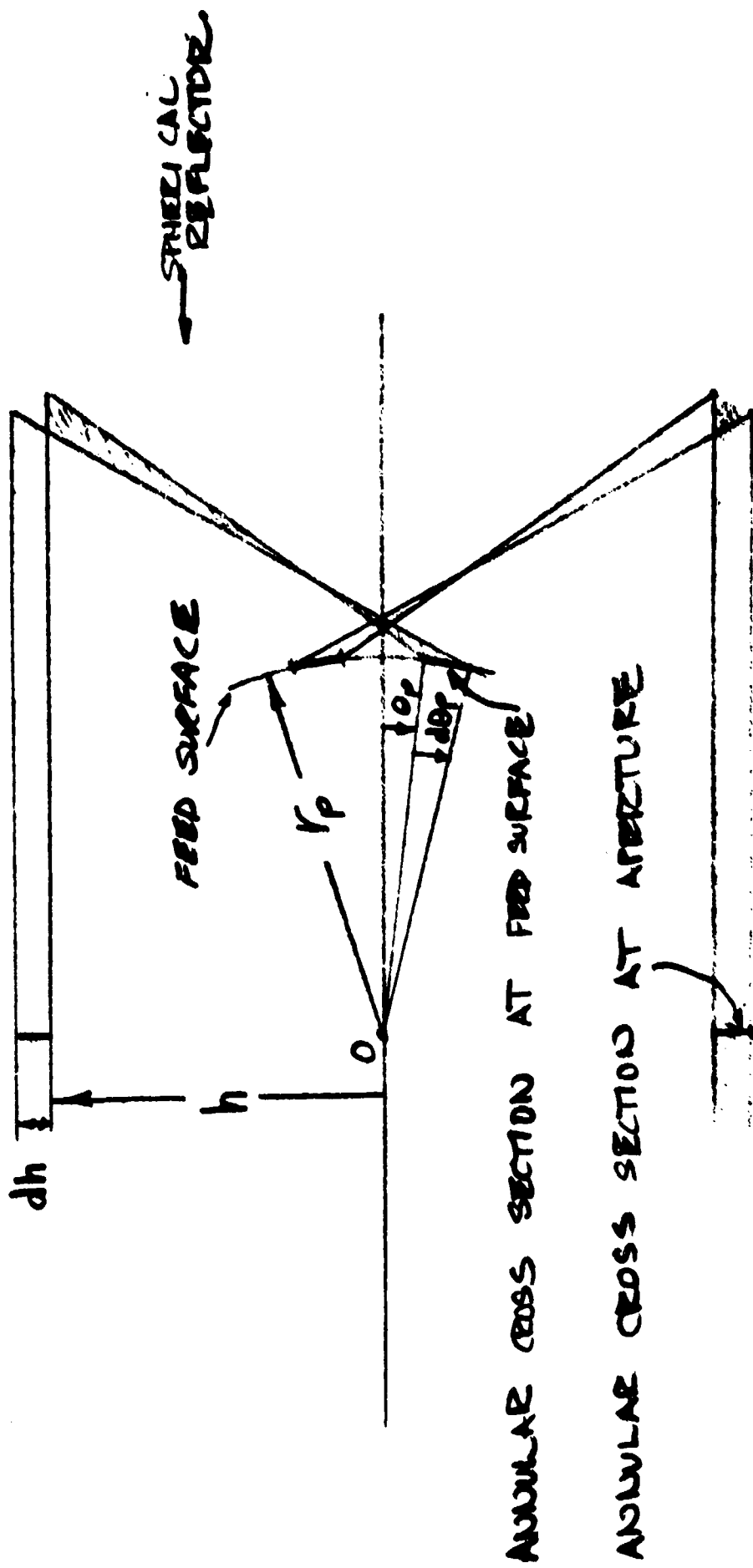


Figure 5. Tubular Pencil of Rays Typical of Ray 3

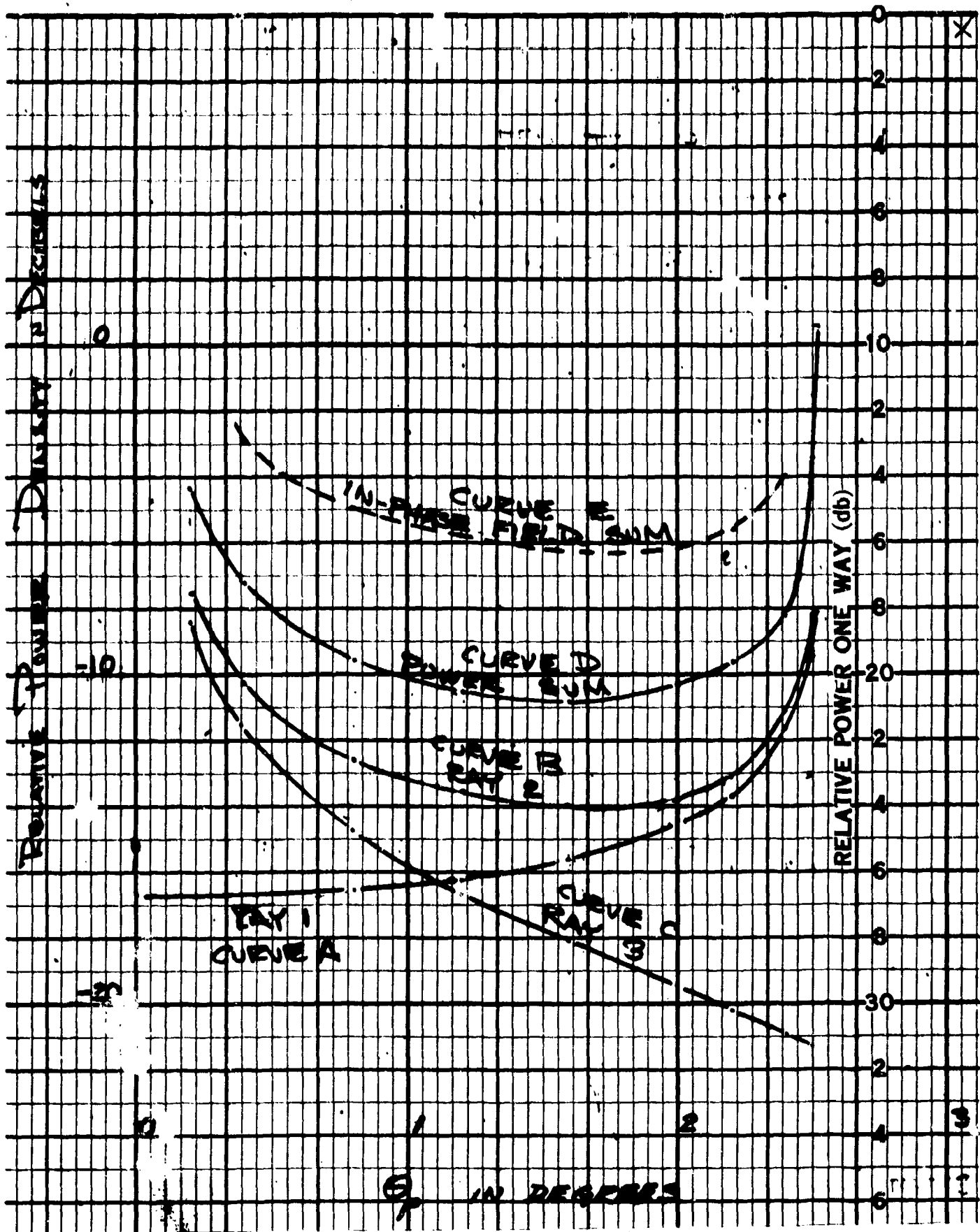


Figure 6. Power Density in the Focal Region Based on Geometric Optics $r_p=0.56$

The relative phase of the three contributions is controlled by path-length as described earlier in References 1 and 3. The θ_p versus path-length curve (Figure 28 of Reference 1) is a particularly useful display of path-length relationships. General expressions for several characteristic dimensions of a generalized curve of this type as functions of r_p are shown in Figure 7.

Dimension s, the arc length of the caustic may be expressed by

$$s = \frac{3}{2} - (3 - 3r_c^2)^{1/2}$$

(This results from combining equations 23 and 24 of Reference 1)

Dimension A, the difference between path-lengths for Ray 3 and Ray 1 (or Ray 2) at $\theta_p = +\theta_c$, is determined from computed tables of these path-lengths because no simple explicit expression for the Ray 3 path-length is known. The near-perfect straightness of the A curve in the logarithmic graph is unexpected because the determination of the data was so involved. Over the range displayed in the figure, however, the curve is described simply by the empirically fitted expression:

$$A = 71 (r_p - 0.5)^{1.856}$$

The other dimensions may be expressed as follows by rearranging known relationships:

$$B = \frac{1}{2r_p} + 2r_p - 2$$

$$C = s - (r_p - 0.5)$$

All dimensions above are normalized with respect to the radius of curvature of the spherical reflector, R.

The rate of change, $dL/d\theta_p$, at the regions of the caustics is of importance in determining beamwidths. Now $dL/d\theta_p = -h$ so that at the axial caustic region where $\theta_p = 0$ for Ray 1:

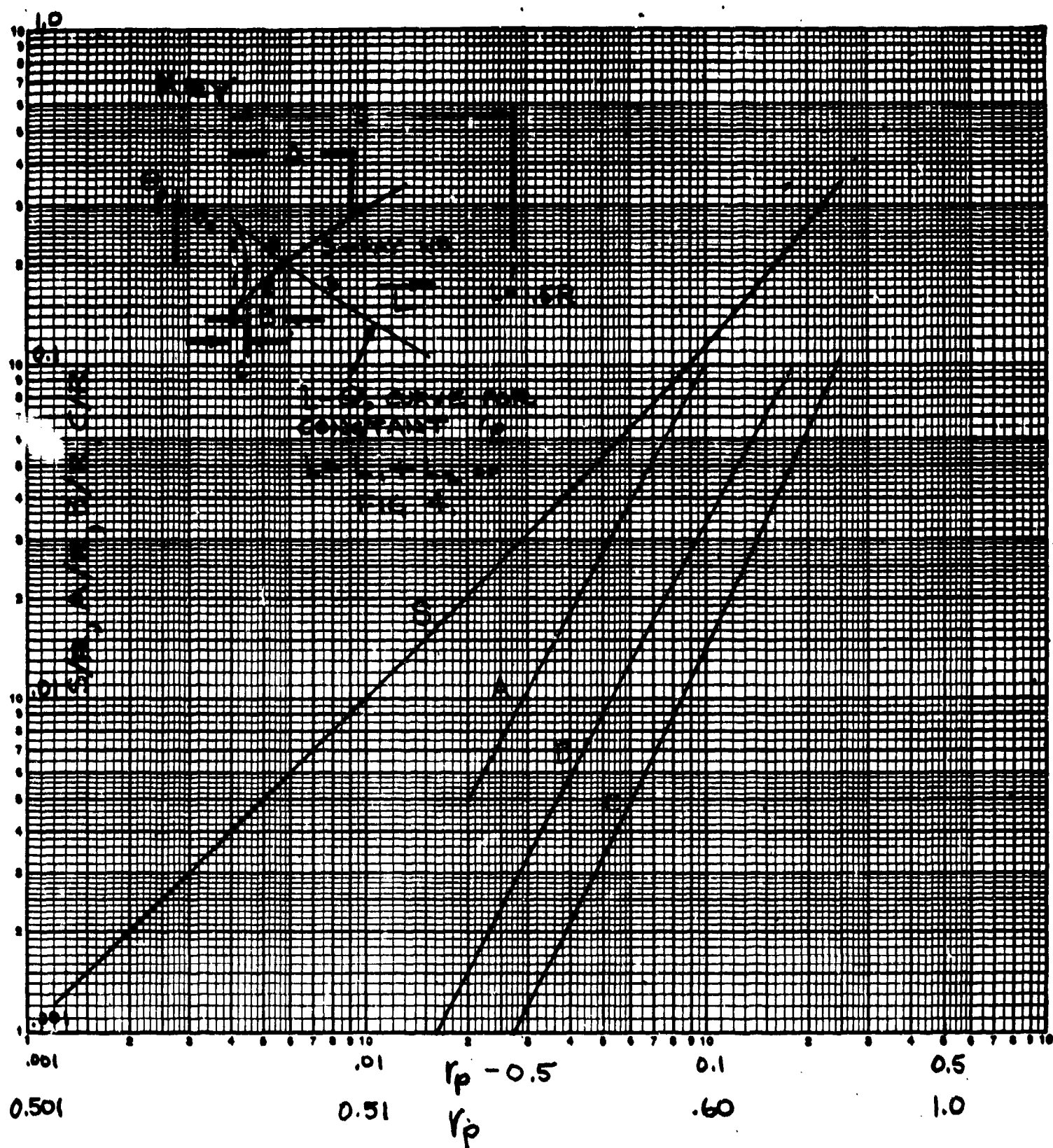


Figure 7. Characteristic Dimensions of $L-\theta_p$ Fishtail Curves

$$|dL/d\theta_p| = 0$$

and for Rays 2 and 3:

$$|dL/d\theta_p| = h_o = \left[(2r_p)^2 - 1 \right]^{1/2} / 2r_p$$

At the caustic surface region $\theta_p = \theta_c$, $r_p = r_c$ and for Rays 1 and 2:

$$4r_c^2 = 1 + 3h^2 = 1 + 3h_c^2 \text{ so}$$

$$|dL/d\theta| = \left[\frac{(2r_p)^2 - 1}{3} \right]^{1/2} = h_c$$

A similar closed expression for h_m , the h of Ray 3 for $\theta_p = \theta_c$, has not been obtained. However, calculated tables show that the total rate of change, $h_c + h_m$, (Rays 1 and 2 vs Ray 3) is equal to 1/1.15 times $2h_o$ within an error of less than 6 percent for r_p values from 0.51 to 0.60.

In the region of the axial caustic the structure of the focal region distribution is dominated by the contributions of Rays 1 and 2 which are strong relative to that of Ray 3 and which are varying in path-length with θ_p at rate h_o in opposite directions for a total relative path-length rate of $2h_o$. The main lobe of the distribution is characteristic of the pattern of a ring aperture and follows the function $J(u)$ where $u = (2\pi h_o R / \lambda) \sin \theta_p$. The first null occurs at $u = 2.4048$ radians. At the null

$$\sin \theta_p = 2.4048 \lambda / 2\pi h_o R.$$

For large apertures $h_o R / \lambda$ is large so $\sin \theta_p = \theta_p$ and the full width from null to null (or minimum to minimum) of the main lobe is

$$2\theta_p = 2.4048 \lambda / \pi h_o R \text{ radians or}$$

$$43.8 \lambda / h_o R \text{ degrees.}$$

The distance measured circumferentially along the surface of the feed sphere corresponding to the null-to-null angle of the main lobe is

$$\frac{2.4048 r_p \lambda}{\pi h_o}$$

Note the independence of this distance with respect to the radius of curvature of the reflector and the dependence only upon r_p and λ .

Lobes other than the main lobe will occur close to the axial caustic if the aperture is large in wavelengths. The null-to-null width of such a lobe is the interval of θ_p required to change the relative path-length by one wavelength or

$$\Delta\theta_p = \frac{\lambda}{2h_o R} \text{ radians or}$$

$$\frac{28.65 \lambda}{h_o R} \text{ degrees.}$$

In the region of the caustic the lobes will be $2h_o/(h_c + h_m)$ times as wide (or 1.15 for r_p from 0.51 to 0.60).

Cross-polarized energy will appear in a $J_1(u)$ distribution which has a null at $\theta_p = 0$ and a null-to-null beamwidth of the first lobe of

$$\Delta\theta_p = \frac{3.8317 \lambda}{2\pi h_o R} \text{ radians or}$$

$$\frac{34.9 \lambda}{h_o R} \text{ degrees.}$$

When the above beamwidth formulas are applied to the case of $r_p = 0.563$ and $R = 140\lambda$ agreement with the method of stationary phase calculations and to the experimental measurements is found to be within about 5 percent in most instances.

This simplified description is least useful in the middle portion of the range of $0 < \theta_p < \theta_c$ because the power density values for the three rays are nearly the same and because the path-length of each ray is varying completely

independently. The number of lobes in this region and the average level may be predicted with useful accuracy, however.

The work reported in References 2 and 3 extends the description of focal region fields beyond the limitations imposed on geometric optics. In that work the effects of polarization are fully accounted for. The induced current on the reflector and the effective current are used to calculate the scattered fields. These fields, expressed by an integral equation, were evaluated by the method of stationary phase using the initial terms of Taylor series expansions, to give first-order correctness. The reader is referred to the cited references for complete detail.

2.4 EQUIVALENCE BETWEEN PATTERNS AND DISTRIBUTIONS IN A SPHERICAL SYSTEM

It is useful to recognize basic relations existing between the (secondary) radiation pattern and the (primary) field or feed distribution in a spherical reflector antenna system.

In the analysis of this section only an all spherical, all concentric reflector system will be considered. Furthermore, the analysis will be limited to those cases in which the diffraction effects at the edge of the reflector are negligible. Obviously it is not valid to neglect edge effects in the general case, however, in most conceivable practical end designs the illumination amplitude at the edge of the aperture is small compared to that of the center portion. Furthermore, for scanning antennas of the subject type for conditions at or near the mid-scan condition the physical edge of the reflector is beyond and remote from even the low-amplitude edge of the usefully illuminated portion of the reflector. Thus, the edge illumination and edge effect are small, or can be made small, for mid-scan conditions in a proper design. Upon this basis rests the validity for neglecting edge effects in this analysis.

It is also assumed that polarization effects are taken into account separately by, for example, the use of elements that are free of response to cross polarization components or by imposing conditions upon the attitudes of the sampling probes and point source.

In a system of specific proportion operating at a specific wavelength and centered upon point O the transmission between P_1 , a point on the feed surface, and P_2 , a point at a semi-infinite distance, depends only upon the angle P_1OP_2 , or θ . This is obvious since the angular attitude of the spherical reflector can have no significance when edge effects are negligible. It is also obvious that θ may be varied in identical manner by moving P_1 or moving P_2 .

It can be stated by application of the principle of reciprocity that if $F_1(\theta)$ is the field spatial distribution function at P_1 for reception from a unit-strength point source at P_2 , and if $F_2(\theta)$ is the field spatial distribution

function P_2 for reception from a unit-strength point source at P_1 , where functions $F_1(\theta)$ and $F_2(\theta)$ include both amplitude and phase, then $F_1(\theta)$ and $F_2(\theta)$ are identical functions, that is $F_1(\theta) = F_2(\theta)$. This includes all effects, such as aberration, diffraction, etc., and is limited only by the stated assumptions. The transmission between point radiators at P_1 and P_2 is independent of the direction of propagation. Therefore, the feed surface field distribution for receiving is exactly equivalent to the secondary pattern (either transmitting or receiving) for a point feed.

A similar but approximate relationship may obtain for a non-spherical system, particularly for one with a focal length long compared to the diameter, over a narrowly restricted angular range. The exactness of the relationship in the spherical case is important as it permits direct calculation of the secondary pattern resulting from any complex feed distribution extending over appreciable angular range. The calculation process may be extremely complex. In many cases it may be impractical.

The function $F(\theta_p, \phi)$ representing the focal region field distribution for reception from a remote point source is theorized upon reversal of sign of the phase angle to become the function approximately representing the feed distribution producing a far-field pattern of a uniformly illuminated aperture. The aperture is concentric with the sphere and has a radius equal to the height, h_1 of the marginal ray. The basis for this theorem is the conjecture that a large section of a wave whose direction of propagation is reversed everywhere along its frontal extent will retrace its previous wave paths. The theorem lacks a rigorous basis, but it is considered to be a useful tool nevertheless.

The experimental transverse feed described in this report supplies partial confirmation of this theorem to the extent that it was designed to establish a feed distribution following the field distribution and to the extent the far field patterns did simulate those of the uniform aperture.

2.5 FEED DISTRIBUTIONS FOR OTHER THAN UNIFORM APERTURE DISTRIBUTIONS

Another important relationship has been found which enables new feed distribution functions to be synthesized which will produce any one of a large group of useful aperture distributions by taking a convolution of the focal region field (Reference 4). For simplicity in explaining this relationship the designation $F_1(\theta)$ will be used for the function describing either the receiving focal region field distribution for an incoming plane wave or the feed distribution producing a uniform plane wave at the aperture. It is understood, however, that these functions differ in the sign of their phase angles. Additionally, it is assumed here again that $F_1(\theta)$ is independent of ϕ_p and of polarization effects.

A feed distribution may be made by superimposing any number of individual $F_1(\theta)$ distributions differing in location on the feed surface by lateral translation (actually translation of the axes of $F_1(\theta)$ in angle to a new origin at coordinates θ_p, ϕ_p) and differing in amplitude and in phase. This discussion is limited to those translated laterally, but all fed in the same amplitude and phase. In this case the resultant aperture distribution is the result of superposition of a number of equal-strength plane waves which are all in phase at the center point of the circular aperture but which are inclined in angle corresponding to the coordinates (θ_p, ϕ_p) .

A most interesting result is obtained when the centers of an infinite number of $F_1(\theta)$ distributions are uniformly spaced around a circle defined by $\theta_p = \Delta$, where Δ is a constant angle. Then the aperture distribution, the superposition of an infinite number of plane wave components each tilted also in angle Δ , is rotationally symmetric and may be expressed simply by:

$$J_0(vr)$$

$$\text{where } v = Rh_{\max} \Delta \lambda / 2 \pi$$

= phase displacement at outer edge of each component plane wave, in radians,

$$\text{and } r = h/h_{\max}$$

= relative radius coordinate.

The normalized pattern function of this distribution may be shown to be:

$$\frac{g(u,\phi)}{g(0,\phi)} = 2 \frac{v J_1(v) J_0(u) - u J_0(v) J_1(u)}{(v^2 - u^2) \Lambda_1(v)}$$

$$\text{where } u = 2 \pi h_{\max} R \sin \theta$$

The aperture distribution efficiency may be expressed by:

$$\eta_{ad} = \frac{[\Lambda_1(v)]^2}{[J_0(v)]^2 + [J_1(v)]^2}$$

Derivation of these expressions is given in Appendix A. Other treatments of the $J_0(vr)$ distribution may be found in References 5 and 6.

A value of $v = 2$ radians corresponds to an edge illumination level of about -13 db and an aperture distribution efficiency of 0.87. The main features of the pattern are:

Half-power point at $u = 1.84$

1/10-power point at $u = 3.16$

First null point at $u = 4.74$

First sidelobe peak at $u = 5.75$

First sidelobe level 0.06 or -24.4 db.

In the more general case the aperture distribution function is the Fourier Transform of the convolution locus. For the $J_0(vr)$ distribution the convolution locus is a circle with an angular radius of Δ . For a $\sin u/u$ distribution in one plane the convolution locus is a straight line. The convolution locus can be a point, array of points, a line, circle, solid area, etc. The amplitude may be tapered and even and odd symmetry may be included for more nearly perfect generality so that the transformation of the original $F_1(\theta)$ for uniform illumination to that for almost any new illumination functions is possible. This method of approach is recognized as being powerful and promises much upon receiving future application in the spherical reflector case.

Sletten et al (Reference 7) have demonstrated effective beam synthesis techniques with specific reference to line source antennas. The possibility is pointed out here of adapting these techniques for the spherical reflector applying them directly for beam shape control in a single plane and by possible extension of development to separate control in two planes.

SECTION 3

EXPERIMENTAL DETERMINATION OF FOCAL REGION FIELDS

3.1 EXPERIMENTAL SET-UP

An experimental set-up was established to obtain corroborative information on the theoretically determined focal region field distribution and to test the performance of a correcting transverse feed. The set-up is the equivalent of a secondary pattern test range comprising a radiating source terminal at one end and a receiving and recording terminal including the spherical reflector at the other (Figure 8).

A 10-foot diameter spherical reflector having a radius of curvature of 5.75 ft., was made available by Air Force Cambridge Research Laboratory. This reflector had been constructed for a study described in Reference 8. This made the construction of a new spherical reflector unnecessary so an active plan to build one of concrete was abandoned. The concrete construction technique is described in Appendix B.

An operating frequency of 24.0 Gc was selected for the experimental work. All tests were made at this frequency. At this frequency the radius of curvature corresponds to 140 wavelengths ($R = 140\lambda$) and the spherical cap having a diameter of 100 wavelengths subtends only 42 degrees at the center of the sphere. Thus, aperture diameters in the range of most practical interest, i.e., well above 100 wavelengths, are available for subtended angles in the range of 60 to 70 degrees.

The reflector is supported rigidly in a fixed attitude with its axis of symmetry directed accurately to the remote source antenna. A test pedestal is affixed to the reflector support structure in such a way that the axis of rotation intersects the axis of symmetry of the reflector orthogonally at the center of curvature of the spherical reflector. The axis of symmetry of the reflector is nearly horizontal and the axis of rotation of the test pedestal is nearly vertical. It is convenient to neglect the small amount of tilt in the following description and to speak of the axis of rotation as a vertical axis and all measurement cuts as horizontal planes. An adjustable extendible fixture attached to the turntable of the pedestal supports a test probe or a feed at any preset combination of height and radial distance from the center of curvature. Provisions are also included for presetting the angle (the "mast head angle") between the probe or feed axis and the radius line to the axis of rotation as well as the angle (the polarization angle) about the probe or feed axis.

Two types of field exploring probes were used. The first is designed to sample either one of the two tangential components of field, i.e., those components perpendicular to the radius vector of the sphere. The radiating

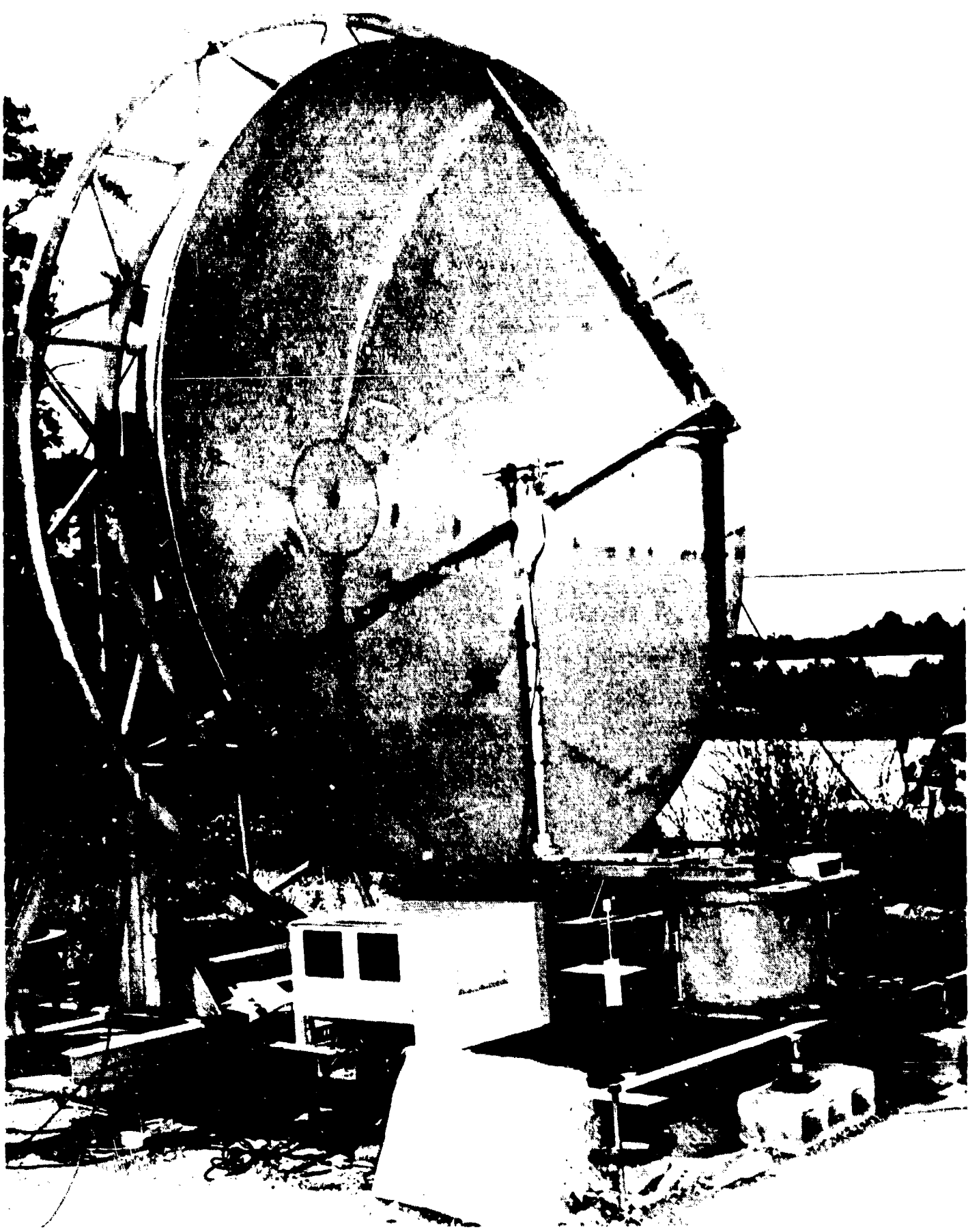


Figure 8. Spherical Reflector at Receiving Terminal With Probe for Sampling Tangential Component of Focal Region Field in Experimental Set Up

NOTE that the bright line of reflected light is due to the machine marks on the surface of the reflector and that its position slightly off the principal axis of the reflector is due to the displacement of the flash bulb above and to the right of the viewing camera.

portion of this probe is the uncovered end of a rectangular waveguide loaded with dielectric material (dielectric constant of 10) and having internal cross-sectional dimensions of 0.15 and 0.30 wavelengths. The measured pattern consists of a broad lobe corresponding closely in the H-plane to the $\cos\theta$ pattern of a short dipole and approximately an omni-directional pattern in the E-plane but decreasing 1 db from the peak at $\theta = \pm 40$ degrees and 2 db from the peak at ± 77 degrees. Thus within the angular region over which the probe receives effective contributions from induced currents in the spherical reflector the probe is a near equivalent of a short magnetic dipole.

The second probe is designed to sample the radial component of electric field. It consists of a thin (0.01 wavelength radius) monopole extending 0.23 wavelength from the center of circular ground plane which has a diameter of 10 wavelengths. The edge of the ground plane is provided with a toroidally curved portion having a minor radius of one wavelength. The measured E-plane pattern within the angular region utilized in the spherical reflector is within ± 1 db of that of a quarter-wave monopole over an infinite plane reflector. This allowable departure of the measured pattern from the ideal is attributable to diffraction at the edge of the ground plane disc.

The source consisting of a klystron oscillator, cavity wavemeter, power supply, power monitor and conventional paraboloidal antenna is mounted at the 100-foot level of a tower 900-feet from the spherical reflector. The antenna is linearly polarized and arranged so that the plane of polarization may be preset by mechanical adjustment to give vertical, horizontal, 45-degree or other polarization. A survey of the field distribution of the received wave in front of the aperture of the spherical reflector indicates that the effect of any spurious path contribution upon focal-region measurements is negligible.

It is necessary to recognize certain differences between the conditions assumed in the theoretical determination of focal region fields and the conditions existing in the experimental measurements. Two principal differences reside in the kind and the attitude of the exploring probe. In the theoretical determination the electric field is resolved into components along the \hat{i} , \hat{j} and \hat{k} directions. This is equivalent to computing the response of small electric dipoles aligned in these directions, respectively. In the experimental work the probe for sampling tangential polarization components is a magnetic dipole, to a close approximation, at least, as far as its response in the direction of interest is concerned. This difference in kind of sampling dipole leads to a difference in the orientation of the resulting field distribution with respect to the polar angle ϕ . The resolution of this difference is accomplished completely by a simple 90-degree change in ϕ . Thus a far-field pattern or focal-region distribution taken in the plane of the exploring dipole is the same for an electric dipole as it is for a magnetic dipole although it is an E-plane pattern (distribution) in the first case and an H-plane pattern in the other. The probe used for experimentally sampling the radial component of field being a short electric monopole, approximates an electric dipole in the directions of interest so no correction needs to be applied in that case.

The movement of the exploring probe in the experimental case is accomplished by rotation about an axis through the center of curvature of the sphere. This affects the attitude of the dipole with respect to \hat{i} , \hat{j} , \hat{k} directions. Therefore, except for the single case wherein the probe dipole axis and axis of rotation are parallel, the probe dipole does not remain parallel to \hat{i} , \hat{j} or \hat{k} direction as θ_p is varied. The departure from parallelism is slight. In the worst case, in which the axis of the probe dipole lies in the plane of pattern measurement, the amount of departure from parallelism is equal to θ_p , the range of which for typical focal regions is $\pm 3^\circ$ degrees or less. Because of the smallness of this departure it is not expected to contribute materially to differences between theoretically and experimentally determined field distributions.

The probe attitude used in experiment is probably a better choice than the \hat{i} , \hat{j} , \hat{k} attitude for any future work as it more conveniently represents the conditions existing at each of the element locations in a multi-element feed array disposed on a spherical surface.

A third difference exists in that all theoretical distributions are computed for plane cuts passing exactly through the principal axis of the system whereas in the experimental setup certain physical asymmetries and uncertainties render this condition improbable. Consequently some distribution features, namely the on-axis nulls for the cross-polarized component of field, may be expected to be modified or obliterated.

3.2 RESULTS OF EXPERIMENTAL MEASUREMENTS

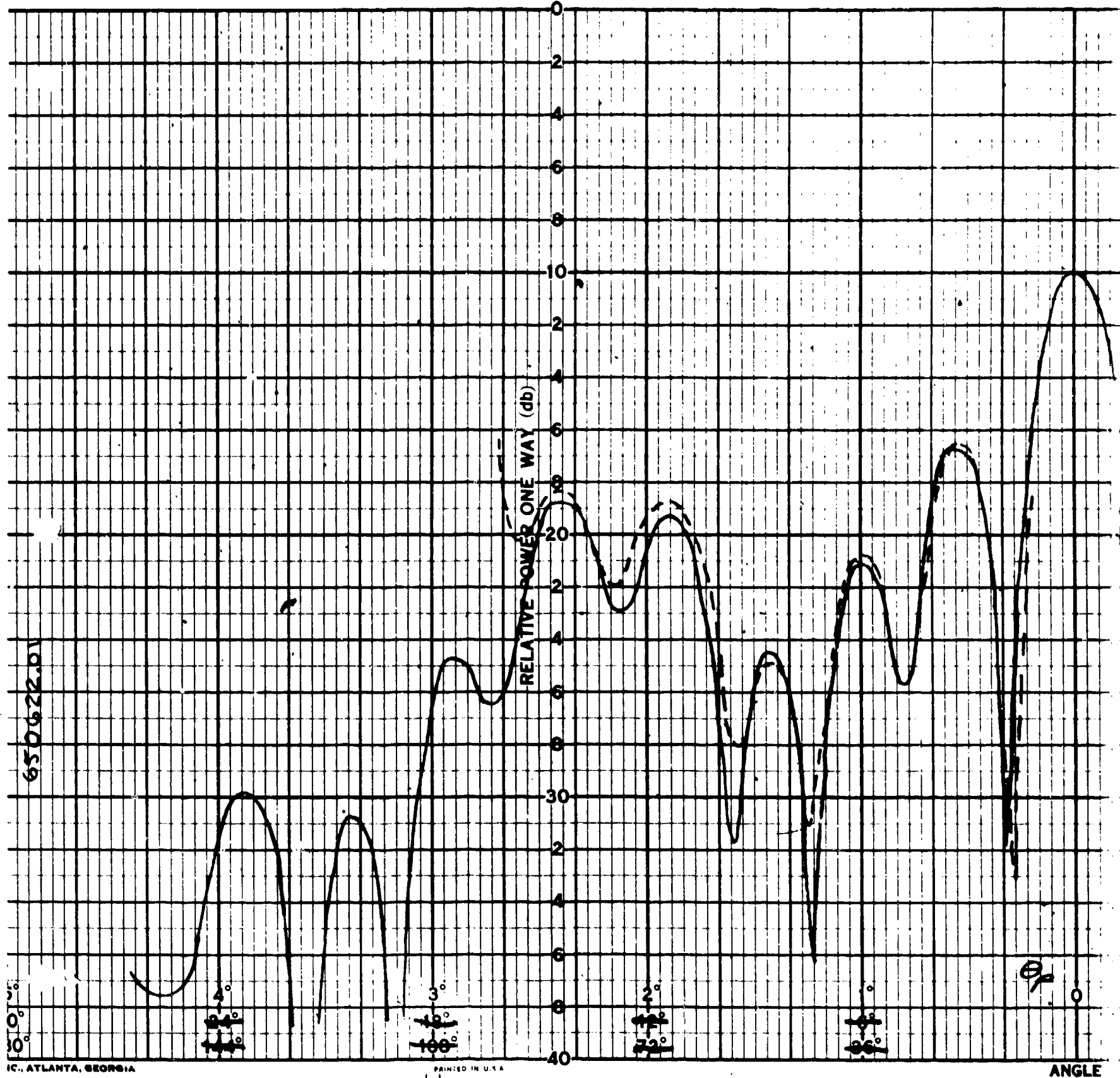
Typical measured focal region distributions in the principal planes are shown in Figures 9 and 10 with corresponding computed distributions. The vertical position of each computed curve has been adjusted to best display the degree of agreement.

In theory there is no response in the principal planes to the tangential cross polarization component. Experimentally the tangential cross polarization response (not shown in the figures) is typically a misshapen replica of the principal polarization response having a peak level 17 to 23 db below the peak of the principal polarization response.

The radial polarization component in the $\phi = 0$ plane is shown in Figure 11 in comparison to the corresponding computed k polarization component.

The experimental and computed distributions for the principal planes exhibit a high degree of agreement in all cases.

Planes other than the principal planes are of special interest as all polarization components have finite response. The $\phi = 45^\circ$ plane typifies the non-principal planes.



A

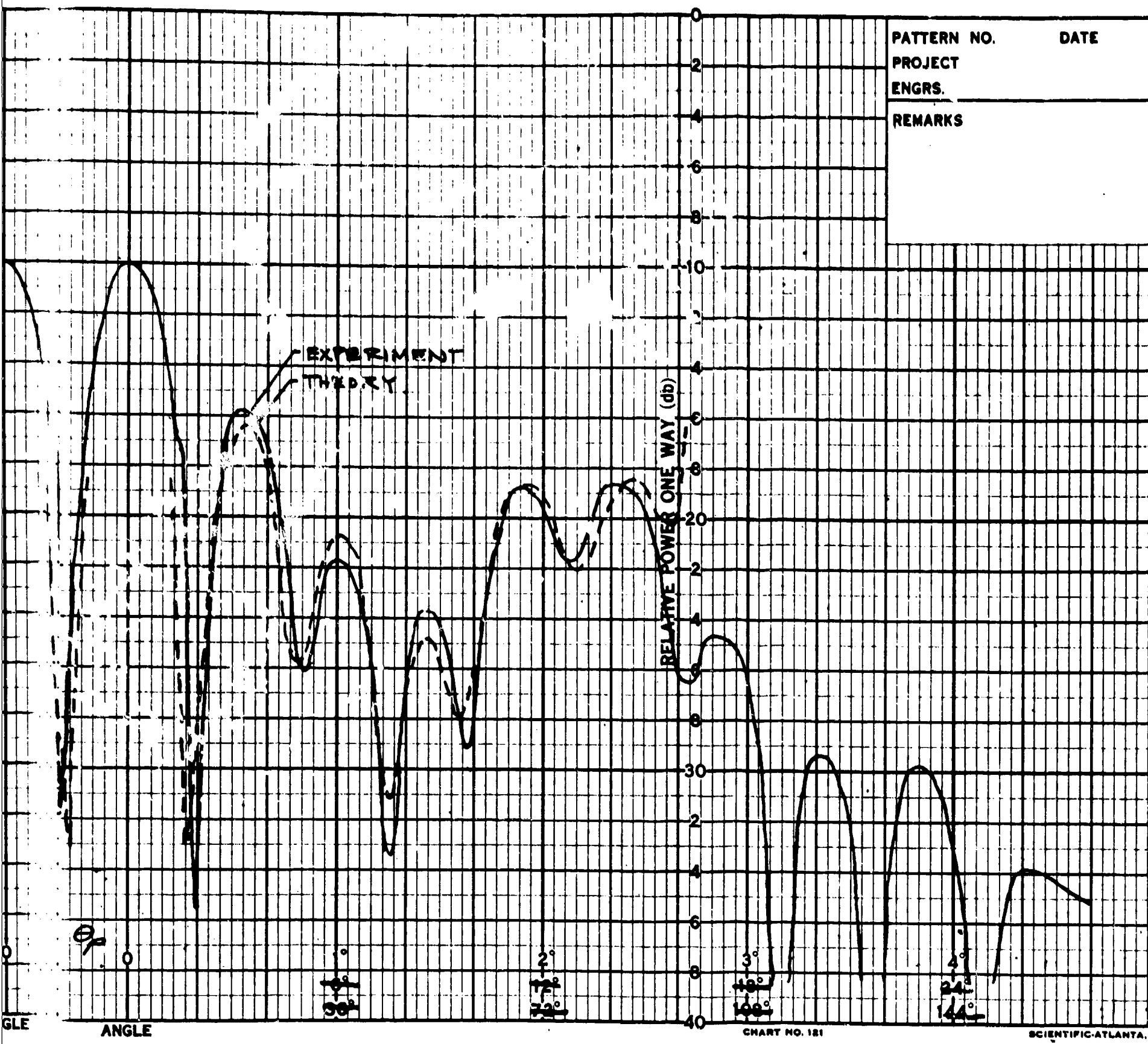
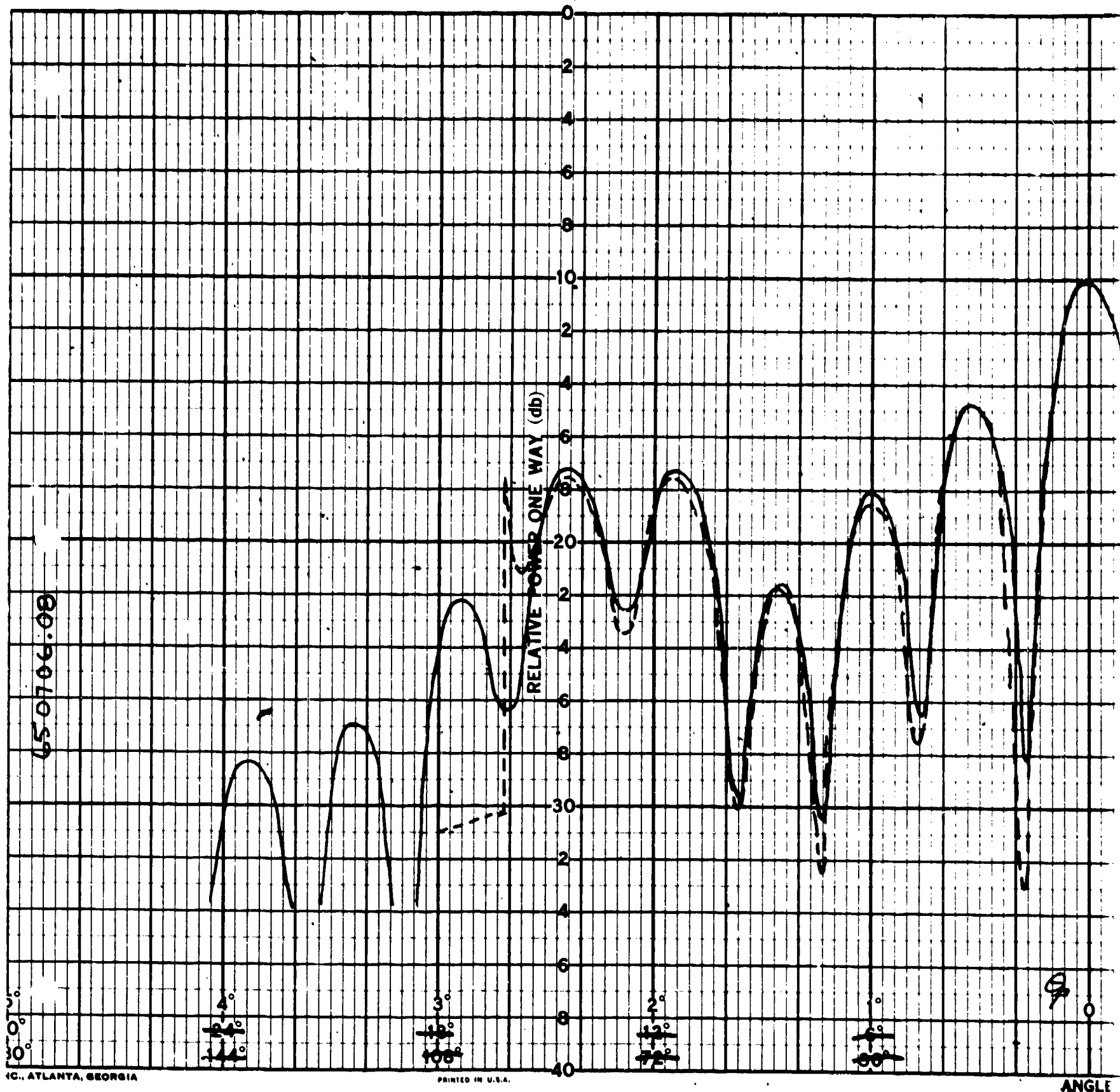
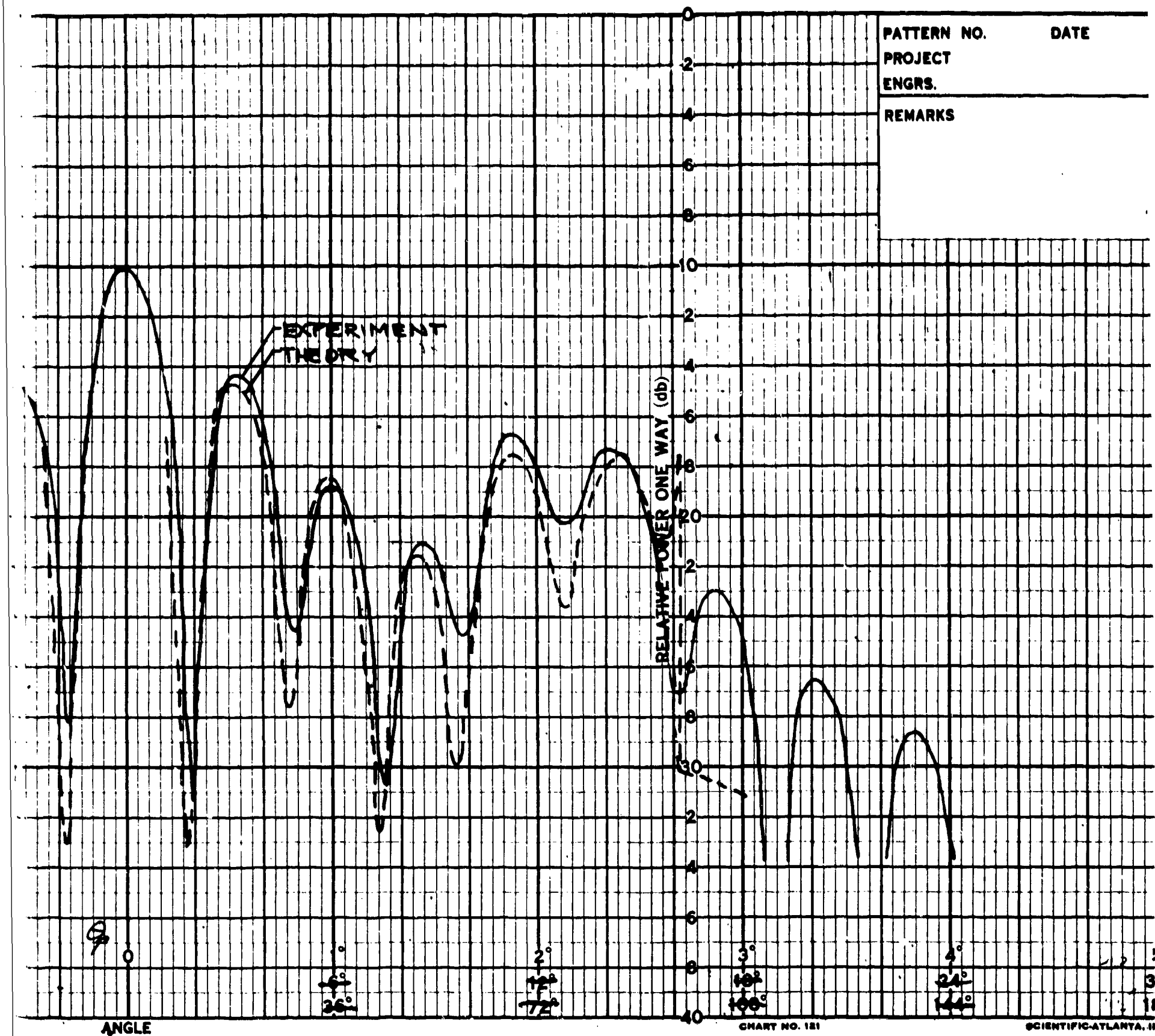


Figure 9. Theoretical and Experimental Focal Region Distribution Taken in Plane of Sampling Dipole for Principal Polarization Component

B

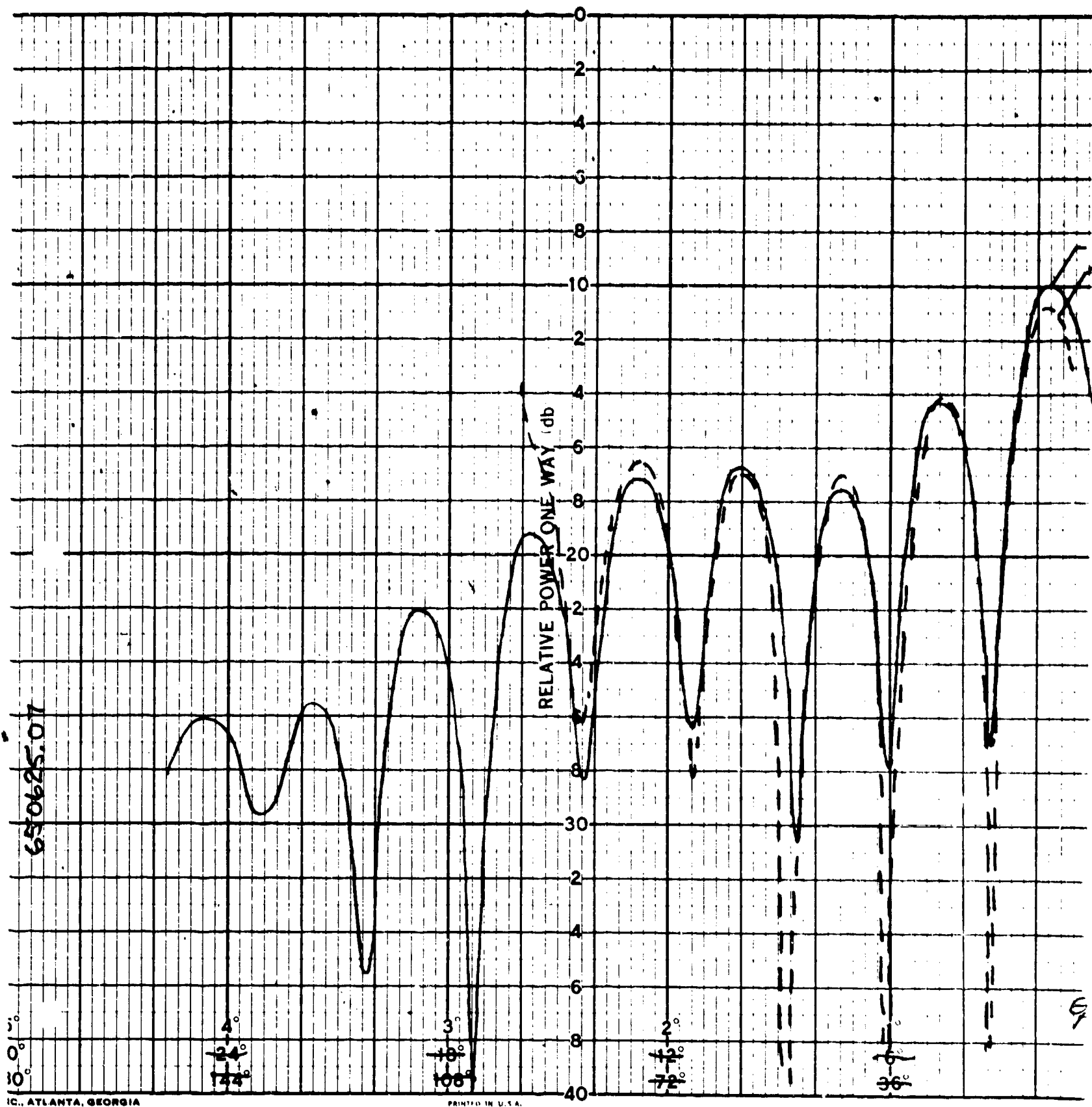


A



B

Figure 10. Theoretical and Experimental Focal Region Distribution Taken in Plane Perpendicular to Sampling Dipole for Principal Polarization Component



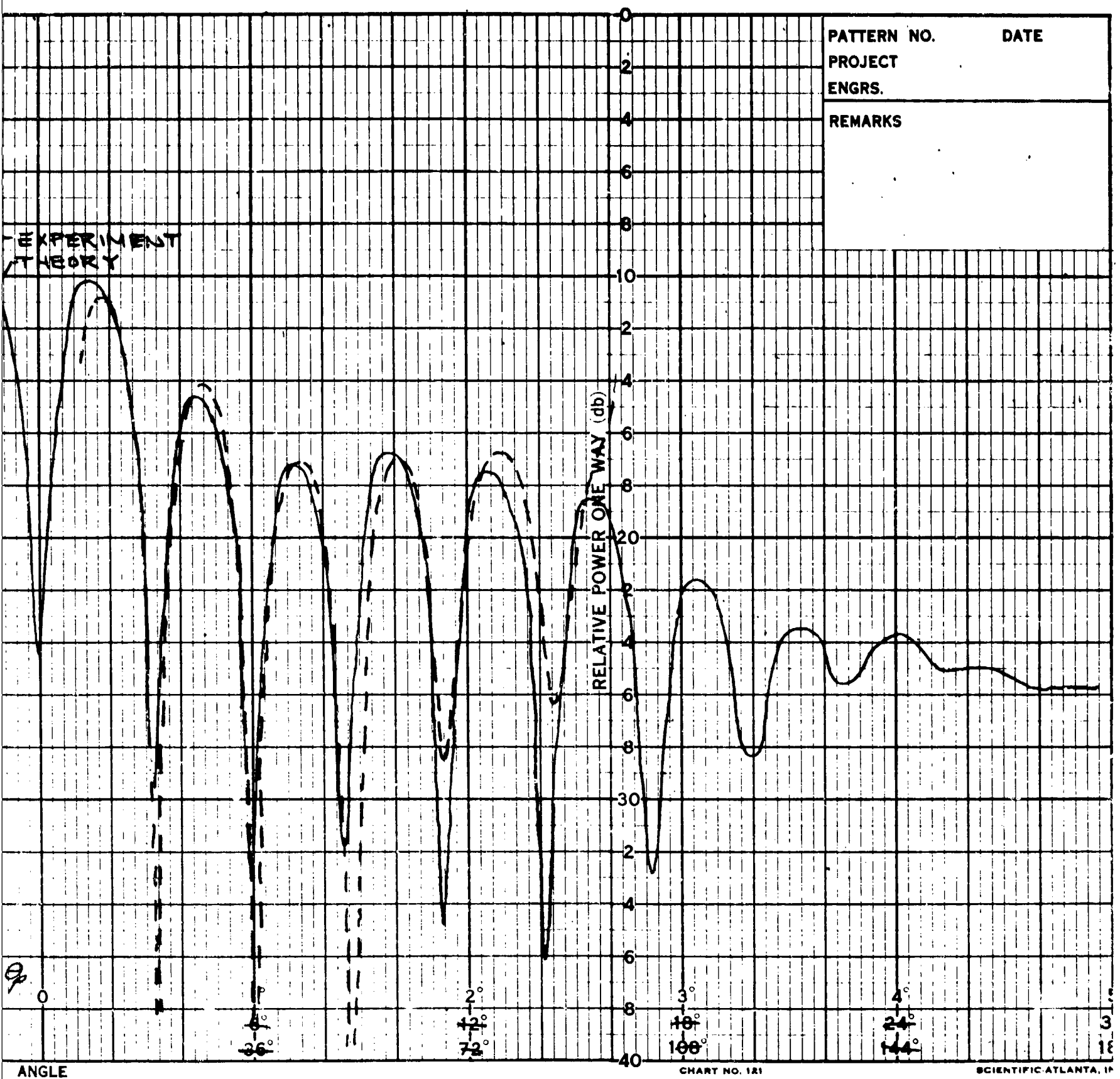


Figure 11. Theoretical and Experimental Focal Region Distribution in $\phi=0$ Plane for \hat{R} and Radial Components of Polarization, Respectively

B

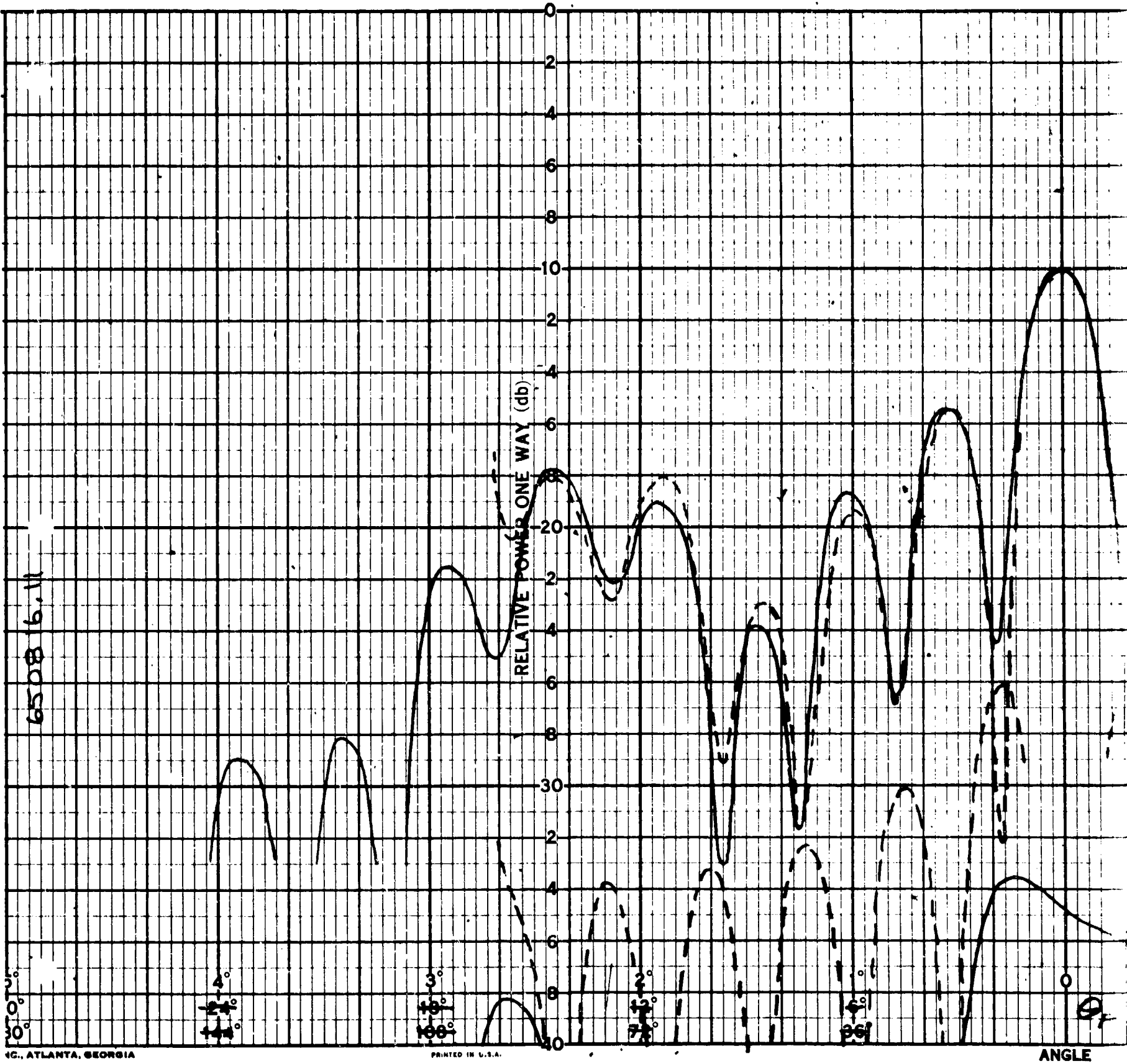
Typical measured focal region distributions taken in the $\phi = 45$ degree plane are shown in Figures 12 and 13 together with corresponding computed distributions.

The measured principal tangential polarization and the computed \hat{i} polarization distributions show good agreement as to overall shape, location and level of lobes and location of minima. The same is true for the measured radial cross polarization and the computed \hat{k} polarization distributions.

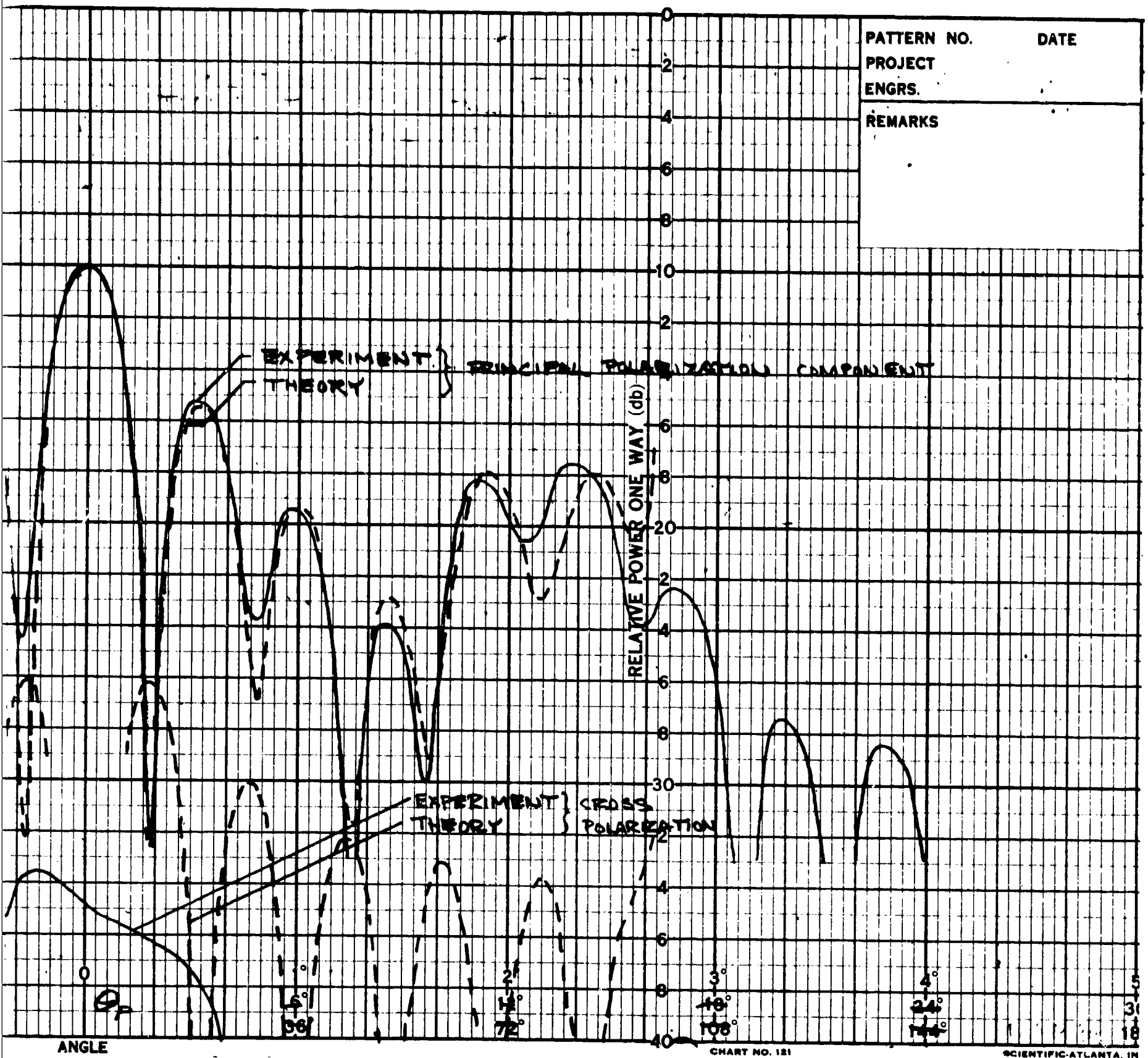
Less complete agreement by far is evidenced by the measured tangential cross polarization and the computed \hat{j} polarization distribution. In this case the amplitude level of the cross-polarized component is known relative to that of the principal polarization beam maxima for both experimental and computed cases. Figure 12 shows these two distributions in proper relative amplitude. The measured level is considerably lower than that indicated by theory. Furthermore, the low level relative to the other two polarization components together with unavoidable slight degree of misalignment and asymmetry can readily account for the irregularity of shape of the measured distribution.

Figure 14 displays the variation with r_p of the lobe maxima levels of the principal polarization component. This variation along with that of the location of the maxima shown in Figure 15 indicates the degree of sensitivity with respect to the radial dimension.

BLANK PAGE

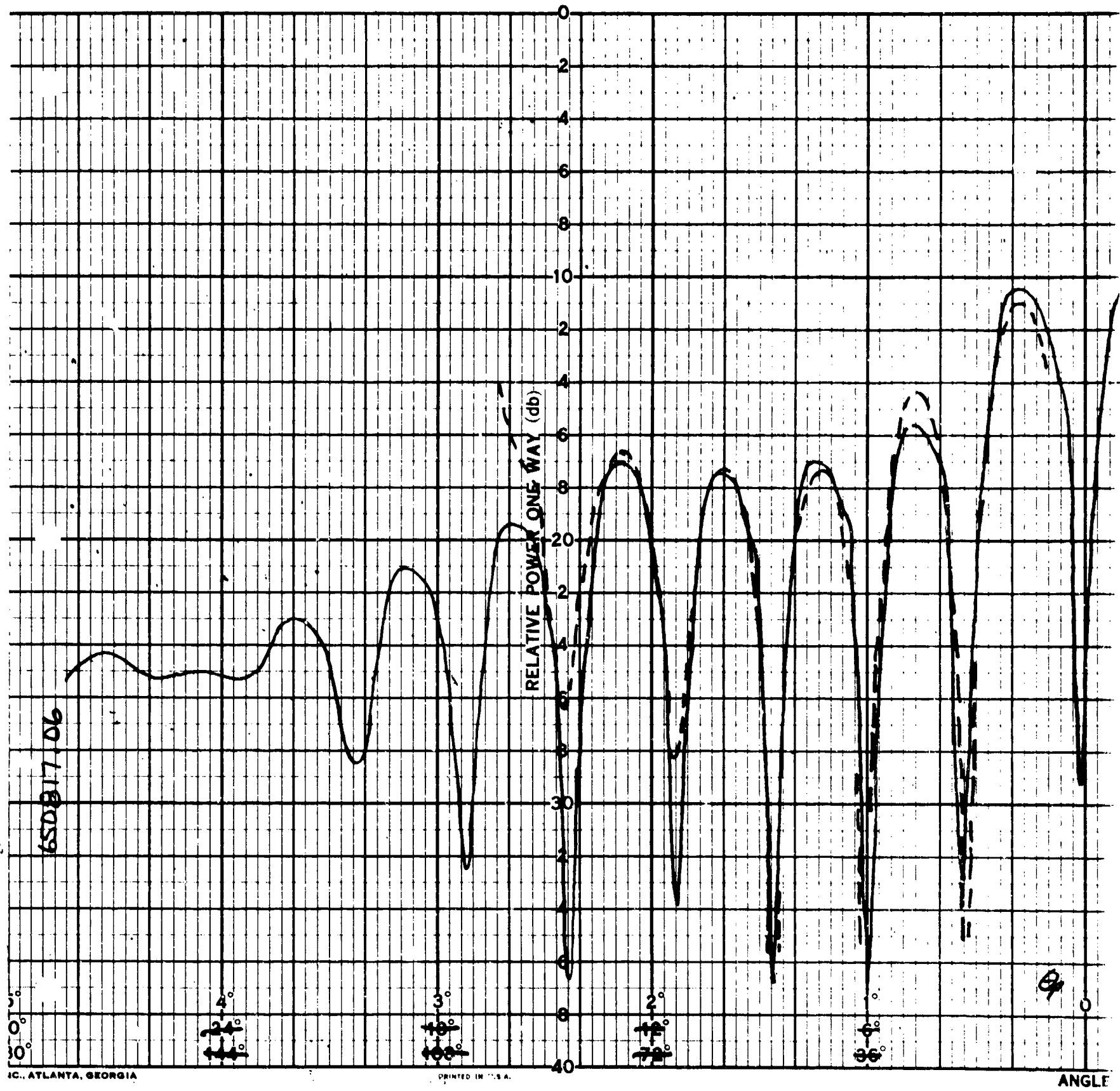


A



B

Figure 12. Theoretical and Experimental Focal Region Distribution in $\theta=45^\circ$ Plane for Principal Polarization and for Tangential Cross Polarization Components



A

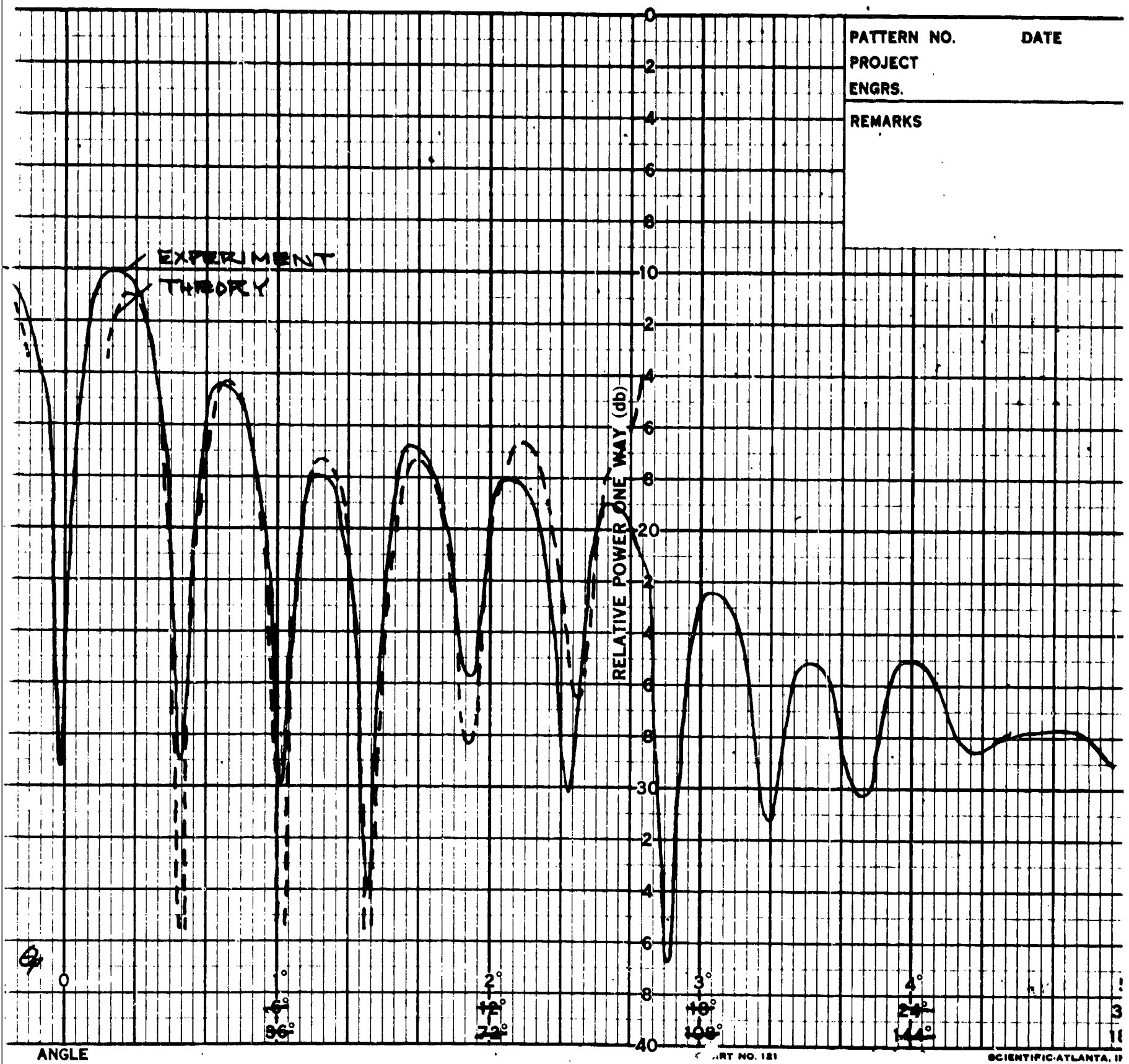


Figure 13. Theoretical and Experimental Focal Region Distribution in $\phi=45^\circ$ Plane for k and Radial Components, respectively

B

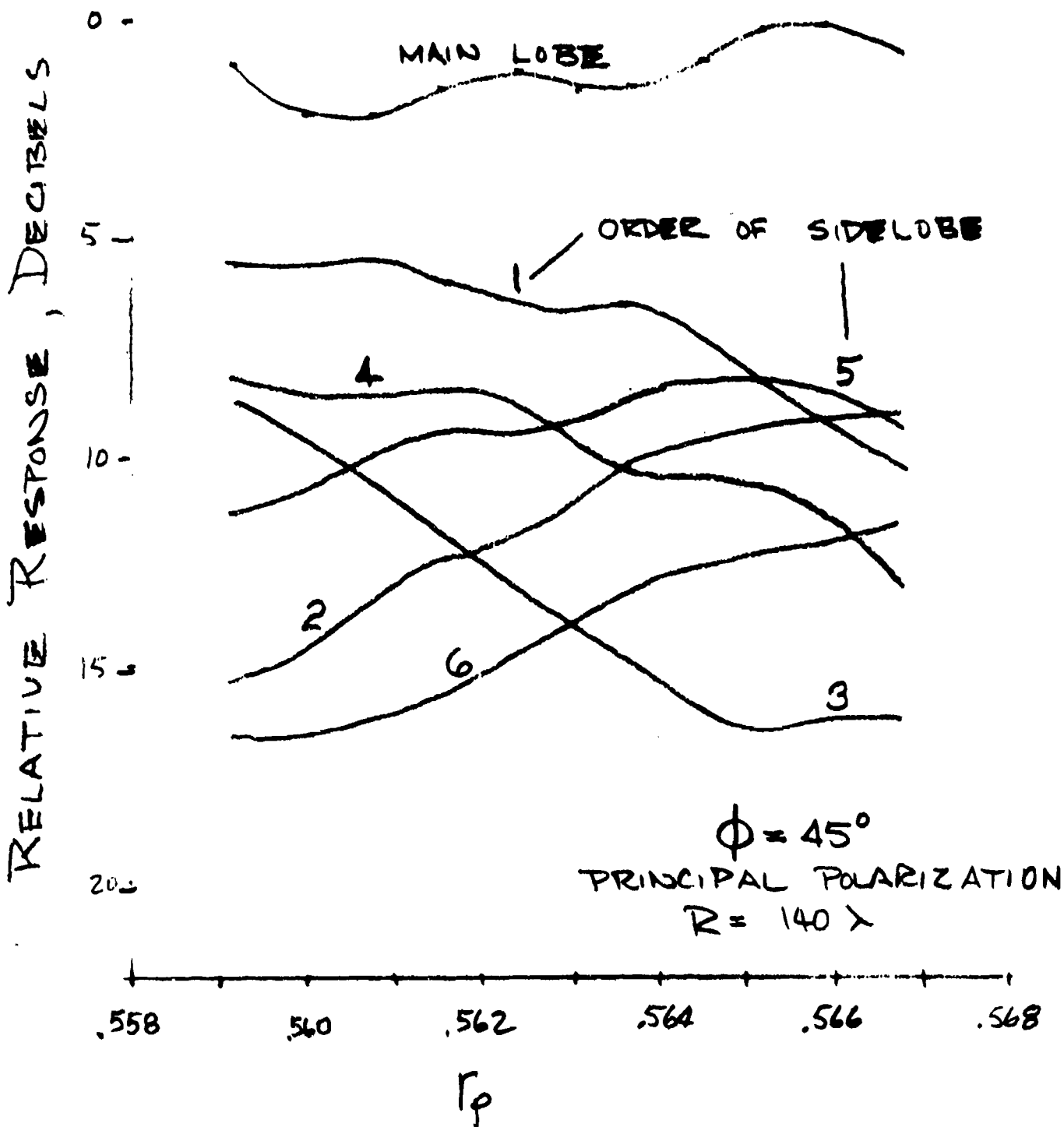


Figure 14. Variation of Sidelobe Level

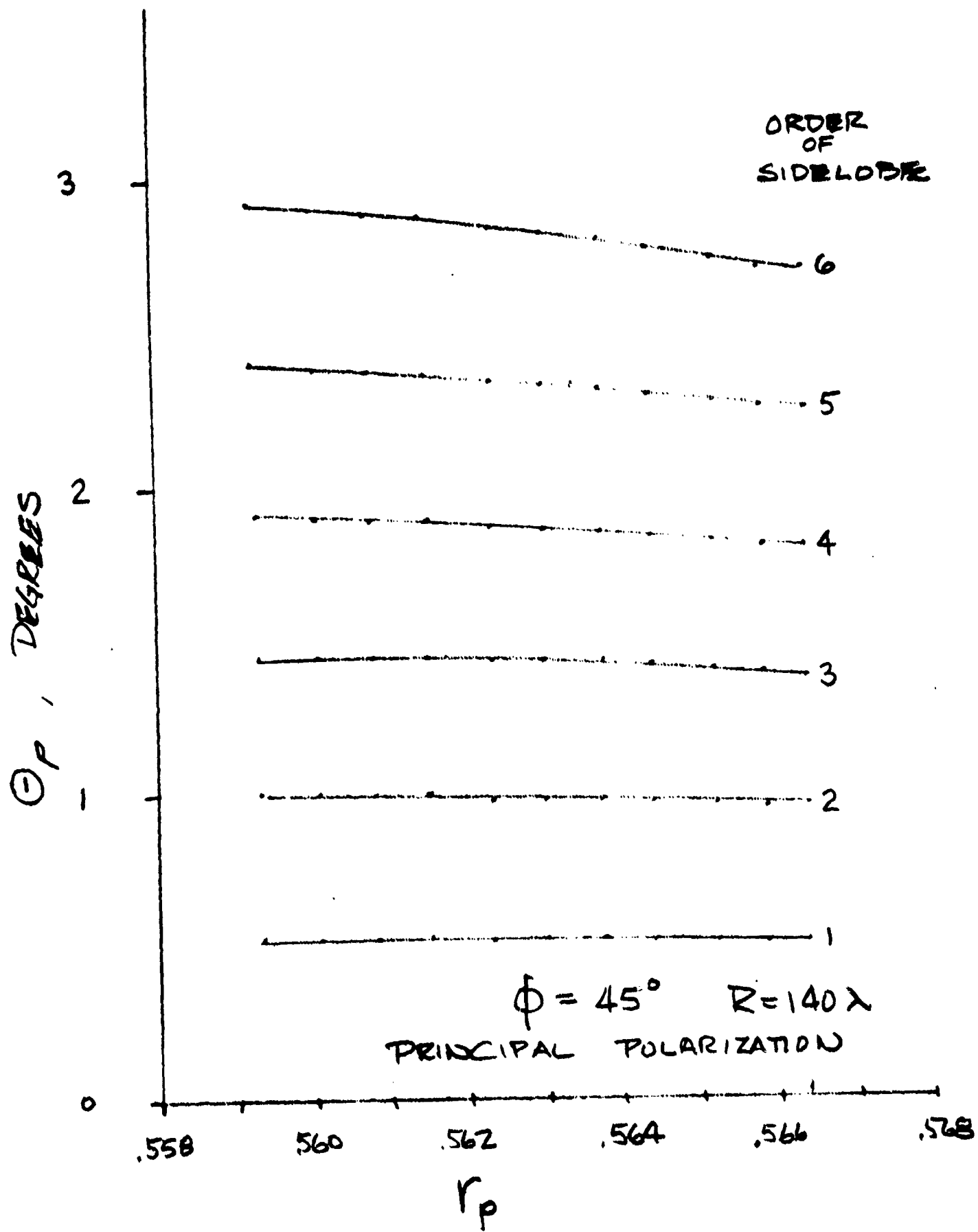


Figure 15. Variation of Sidelobe Angle

SECTION 4

AN EXPERIMENTAL TRANSVERSE CORRECTING FEED

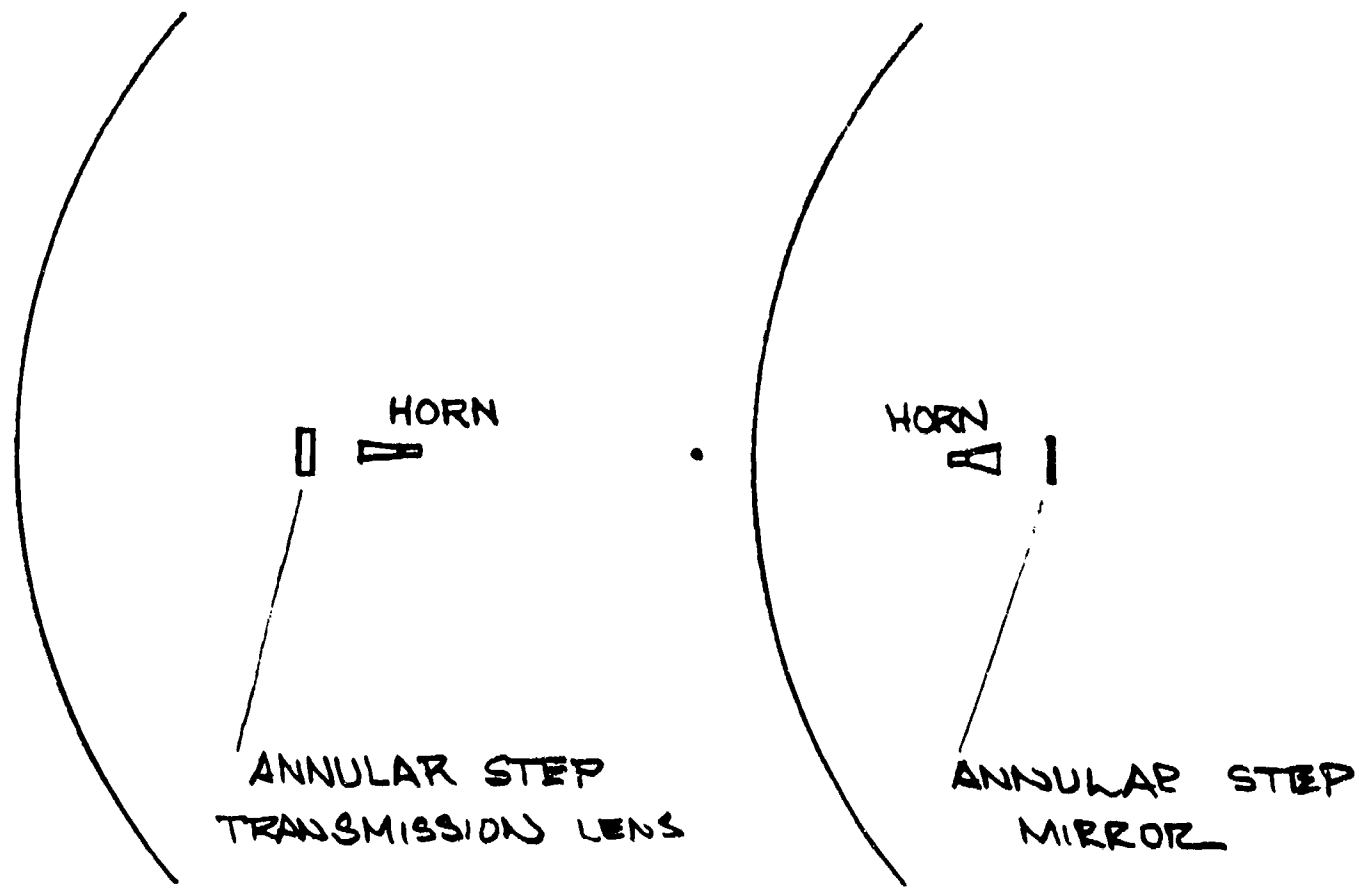
4.1 SELECTION OF REFLECTING TYPE ANNULAR STEP DISC FEED

An objective was established to utilize the knowledge of focal region fields gained from the preceding theoretical and experimental work in the design of an operating model of a transverse correcting feed. It was desired that the feed be capable of demonstrating the achievement of uniform amplitude aperture distribution when illuminating a wide angular portion of the test sphere at 24 Gc.

Thorough consideration was given to several factors prior to the selection of the type of feed to be used. An array feed would be representative of future feeds to be designed for electronic beam control. For this reason it was desirable that the experimental feed be of the array type having a number of radiating elements excited by a feeding network. However, the formidable problems associated with the successful execution of a working model of an array feed operating at 24 Gc were judged to weigh too heavily against use of the array as the initial experimental feed. A more suitable general type appeared to be the annular step disc feed, to be described below, a version of which was selected for the experimental feed.

The principle of the annular step disc feed (ASDF, for short) is illustrated by Figure 16. A small radiator, a horn for 24-Gc design, illuminates a circular area in the focal region of the spherical reflector. The second element of the ASDF is placed to coincide with this area. This disc-shaped element may be a transmission element (a lens) or a reflecting element (a mirror). In either case the element is fashioned with concentric annular zones which introduce stepwise radial variation of phase to the wave contributions leaving the disc in the direction of the spherical reflector. The phase steps are dimensioned to be equal and opposite in effect to the phase characteristic due to the spherical aberration. Thus, when the amplitude distribution across the "output" surface of the disc is made to correspond closely to the required characteristic a completely corrected feed is the result. In practice, the required amplitude characteristic is approximated only in overall shape or envelope and details of the amplitude characteristic are not reproduced.

The transmission type ASDF may employ lenses of natural dielectric, artificial delay medium, path-length medium, metal-plate waveguide medium or some combination of these. (See Reference 9 for lens terminology used here.) The steps in phase may be provided by steps in lens thickness. This method is similar to that used in conventional zoned lens design except that adjacent zones in the ASDF differ in phase by approximately 180 degrees. Alternatively, the phase steps may be provided by variation of the refractive index within



A. TRANSMISSION TYPE

B. REFLECTION TYPE

Figure 16. Annular Step Disc Feeds

the lens, or by controlling the electrical path length in some other way. For example, a metal-plate lens of the egg-crate type may be fitted with dielectric phase-shifting inserts of graduated effective phase shift. This technique is attractive for future application wherein time modulation of the phase shifter elements can be exploited for obtaining desired rapid antenna beam control. However, formidable problems seem to rule out the use of this type or any other lens except a natural dielectric lens for experimental work at a frequency of 24 Gc.

The transmission type ASDF has the advantage that the horn does not block the wave leaving the output side of the lens. Horn energy can be constrained from spilling over the edge of the lens by the addition of a conical metallic shroud which may also be used as a mechanical support.

The design of a transmission type ASDF must include consideration of the strong and variable effect on transmission coefficient at the "output" surface of the lens attributable to the wide range of angle of incidence of the rays leaving the lens. Each spot on the output surface of the lens is intended to contribute radiation components in three different ray directions at once. It is apparent that the adequate control of the transmission and reflection coefficients at this surface cannot be attained without extensive development.

The reflection type ASDF offers the most straightforward and satisfactory approach to attainment of the objective established for the experimental program. The phase correcting mirror is simply a metallic disc with annular steps machined into the active face. No dielectric material is used; propagation of the wave beyond the aperture of the horn is under free space conditions.

Control of optical ray lengths is attained solely by control of physical dimensions of the mirror surface. At 24 Gc these dimensions may be controlled to within a few thousandths of a wavelength. For these reasons the reflection type of ASDF was selected for the experimental feed. An additional advantage, the inherent functioning of the ASDF in almost automatically providing the equivalent of Huygens-source or plane wave radiation, was recognized later (see discussion of polarization in Section 5).

4.2 BASIS OF DESIGN OF EXPERIMENTAL FEED

The experimental feed is designed to illuminate the area enclosed by the circle of least confusion at a relative radius r_p of 0.563. At this radius the relative height of the marginal ray is 0.5 so that the diameter of the circular aperture defined by all marginal rays is equal to the radius of curvature of the reflector. The nominal illuminated aperture of the experimental antenna system is thus 5.75 feet or 140 wavelengths at 24 Gc.

A horn and an annular step mirror are proportioned to establish over the circle of least confusion the best approximation to the principal polarization component of the computed focal region field with a reversal in sign of the phase angle. The amplitude and phase of the \hat{I} -polarization field distribution computed for $\theta = 45$ degrees was accepted as the ideal radial distribution for all values of θ in the experimental feed.

The selection of the horn and the focal distance between the horn and the $r_p = 0.563$ feed surface was made to achieve several objectives. A distribution of illumination across the face of the mirror approximating roughly the envelope of the computed amplitude is desired while, at the same time, a high spillover efficiency is desired. The horn aperture is to be large enough to provide a near equality between E and H-plane patterns and a fair impedance match while small enough that the mirror is in the far field of the horn. The focal distance is to be large enough to avoid blocking of the marginal rays by the horn and yet be near the optimal length that results in the least departure of the mirror from the surface of the r_p sphere.

The feed horn has a circular aperture of 0.531 inches (1.08 wavelengths) fed in the TE_{11} mode by a long nearly-conical taper section from 0.170×0.420 -inch waveguide. This horn has E-, H- and 45° -plane main lobe patterns that are practically identical. The measured 10-db beamwidth of each is 104 degrees. With this horn located at a focal distance of 4.18 wavelengths from the r_p sphere the edge of the mirror intercepts the horn pattern at the -6.2 db level. This corresponds to an estimate of 76 percent of the energy in the lobe impinging on the stepped mirror or a primary spillover efficiency of -1.2 db. A space taper of -2.4 db combines with the pattern taper to effect an overall illumination taper at the edge of the mirror of -8.6 db relative to the center of the mirror. A plot of the illumination of the impinging wave is shown in Figure 17 together with theoretical curves for comparison.

At the focal distance chosen the horn does not block the marginal rays. The horn aperture unavoidably does block the paraxial rays. A small obstacle at the location of the horn aperture will produce an optical shadow 5.4 times its size at the "vertex" of the sphere on an optical basis. This is almost negligible. However, the actual shadow and surrounding diffraction disturbance will be greater at the operating wavelength and can be expected to have an appreciable effect.

The design of the annular steps in the mirror was performed by constraining the path length of the horn-to-mirror rays to compensate for the path length equivalent of the phase characteristics of the computed focal region field. The mirror is divided into five concentric annular zones and one central circular zone. The annular mirror surface zones are conical. The element of the cone for each annular zone is determined for two design points corresponding closely to the θ values at which the computed field intensity level is $-n$ db from the peak level for that zone. For the inner zones n is taken at 3 db but for the outer zones a better phase fit was found to exist for smaller n 's (down to 1 db). The central circular zone is plane. It is

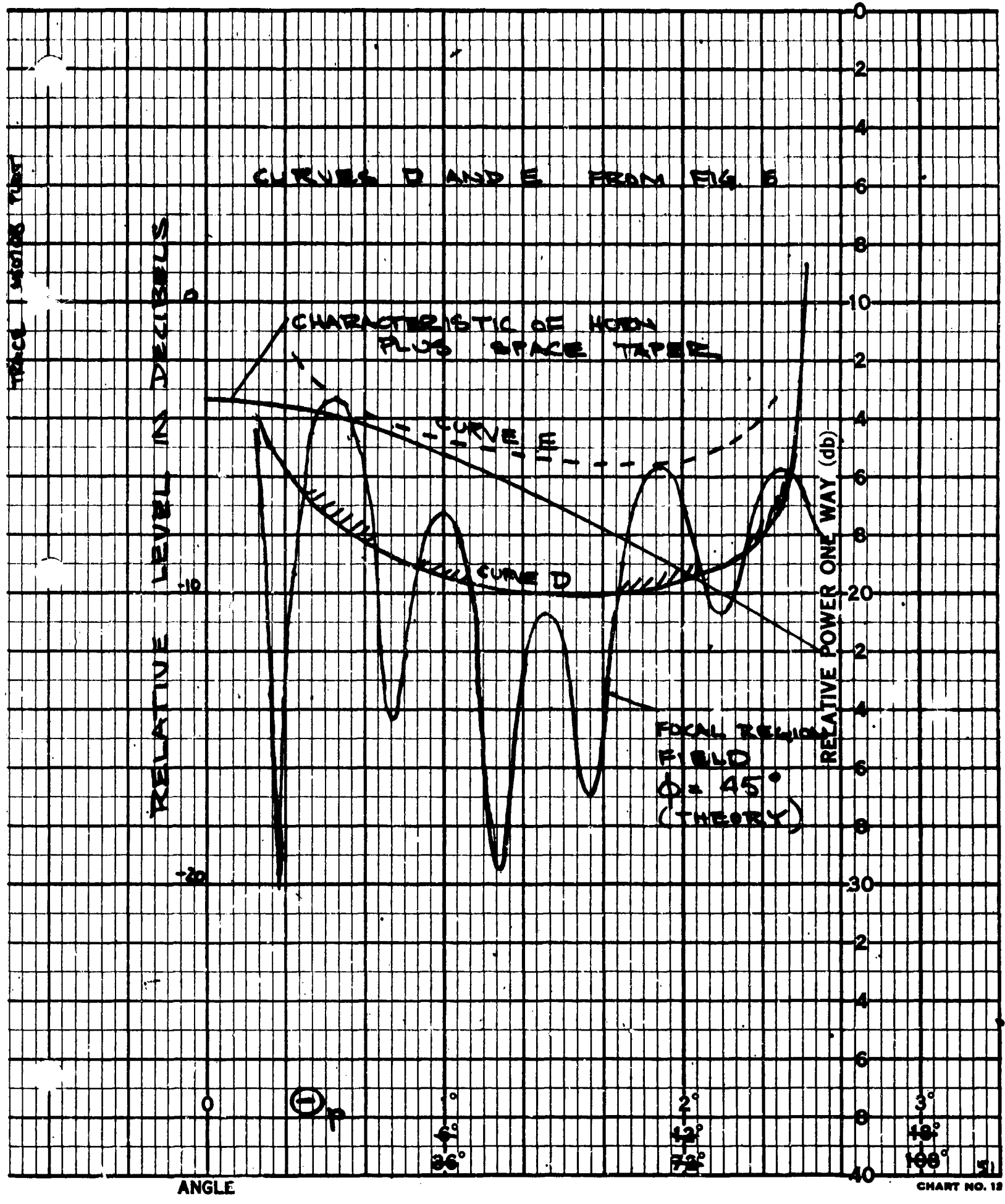


Figure 17. Illumination of Annular Step Mirror

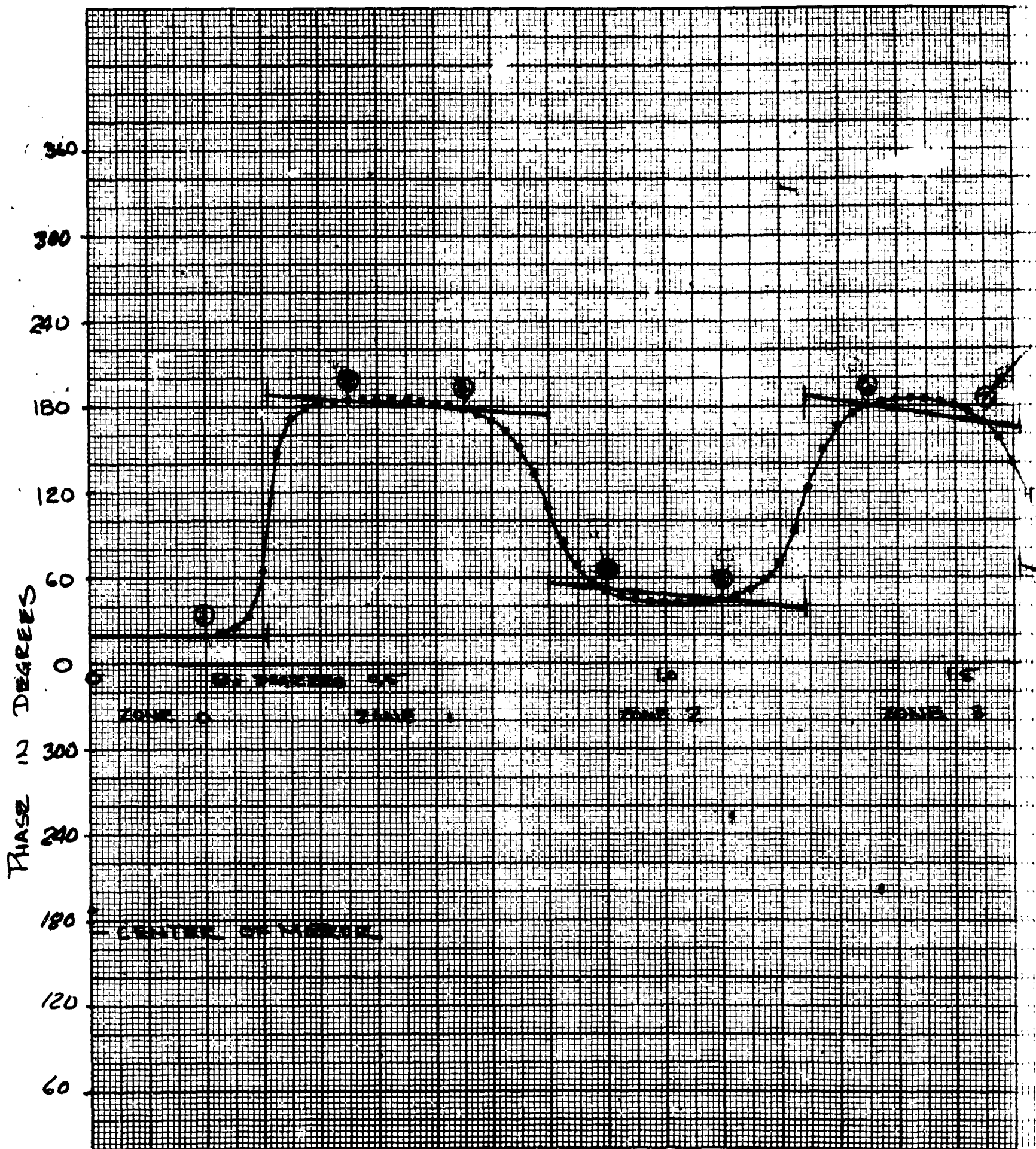
determined for a single design point corresponding to $\theta_p = 0.2$ degrees. The interface radii between adjacent zones corresponds to the θ_p value at which the field intensity reaches a minimum. The design points for the zones are shown relative to the computed phase in Figure 18. At these points the phase compensation is nominally correct. For other points the error in phase compensation may be estimated from the departure of the straight lines (representing zones) from the computed phase points.

A cross-section of the mirror for the ASDF is shown in Figure 19. The axial hole was provided for alignment and centering use. It has no electrical function. The diameter of this hole, 0.38 wavelengths, is small enough to avoid any electrical effect due to its presence in the center of the zeroth zone. The departure of the mirror surface from the $r_p = 0.563$ sphere is a maximum of 0.182 wavelength. The design was adjusted so that a balance was maintained between the maximum positive and negative values of this departure. As a result, all points on the stepped mirror lie between the two spheres defined by $r_p = 0.5630 \pm .0013$. This was accomplished, in part, by setting the total path length for the zeroth zone and for the fifth zone to differ from the total path length for the other zones by -1 and +1 wavelengths, respectively. The term total path length is used here to describe the composite of (a) the path length from the horn to the design point plus (b) the path length equivalent of the phase angle of the computed focal region field. (Since the field at any one point in the focal region, in general, is the resultant of waves arriving from three different directions over wave paths differing by many wavelengths the absolute length of the path component (b) above has no major significance.)

Figure 20 shows the horn and stepped mirror of the experimental ASDF. The rigid bracket supporting the horn from the edge of the mirror is shown. The feed is held in the experimental set-up by an attachment at the back of the mirror which can be preset to place the plane of the horn support at an angle of 0, 45 or 90 degrees with respect to the plane of the pattern measurement. The horn can be preset in its supporting clamp at any desired angle of polarization with respect to the plane of the horn support. It may be noted that one plane cutting the axis of the feed coincides with the split in the horn support clamp and that the major portion of the horn support lies to one side of this plane.

4.3 EXPERIMENTAL EVALUATION OF ASDF

The test set-up described in Section 3.1 was used with minor changes to measure the patterns of the spherical reflector excited by the ASDF. A fixed attenuator pad (19.4 db) was placed between the feed and the mixer unit of the receiver to avoid non-linearity of response due to signal overload of the mixer. A calibrated variable attenuator was inserted in the source antenna feed line to provide accurate measurement of level difference.



A

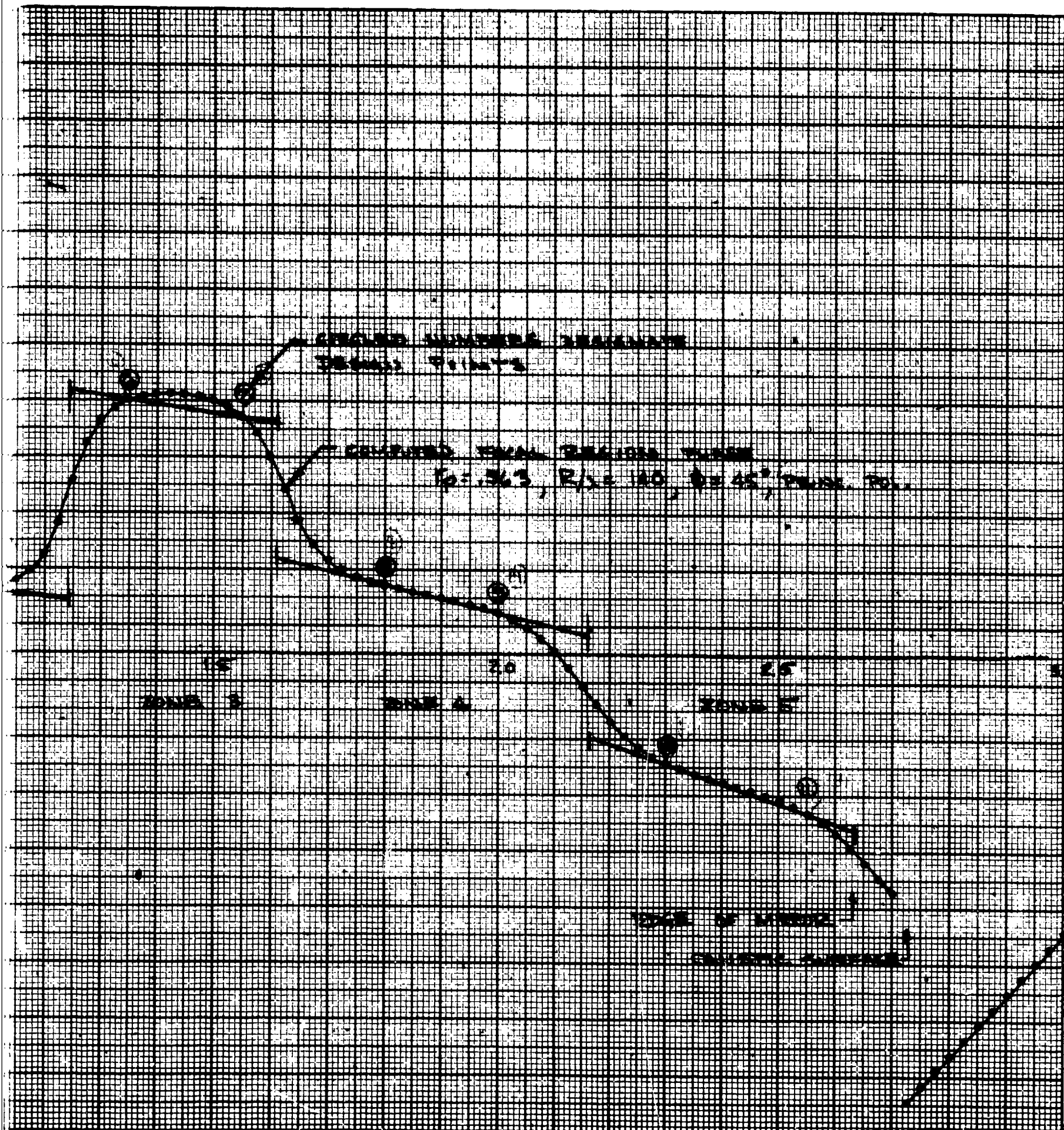


Figure 18. Phase Design of Experimental Feed

B

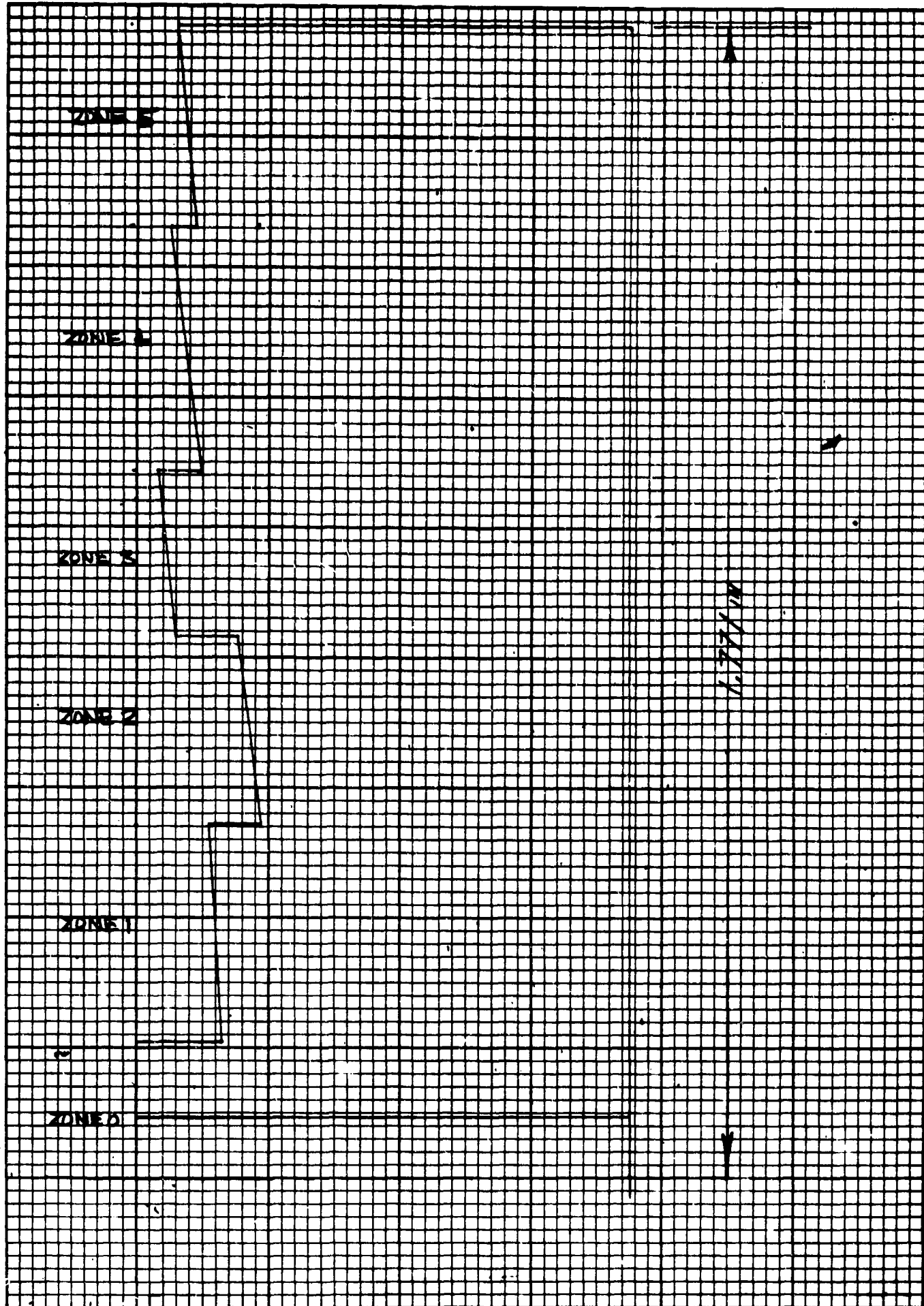
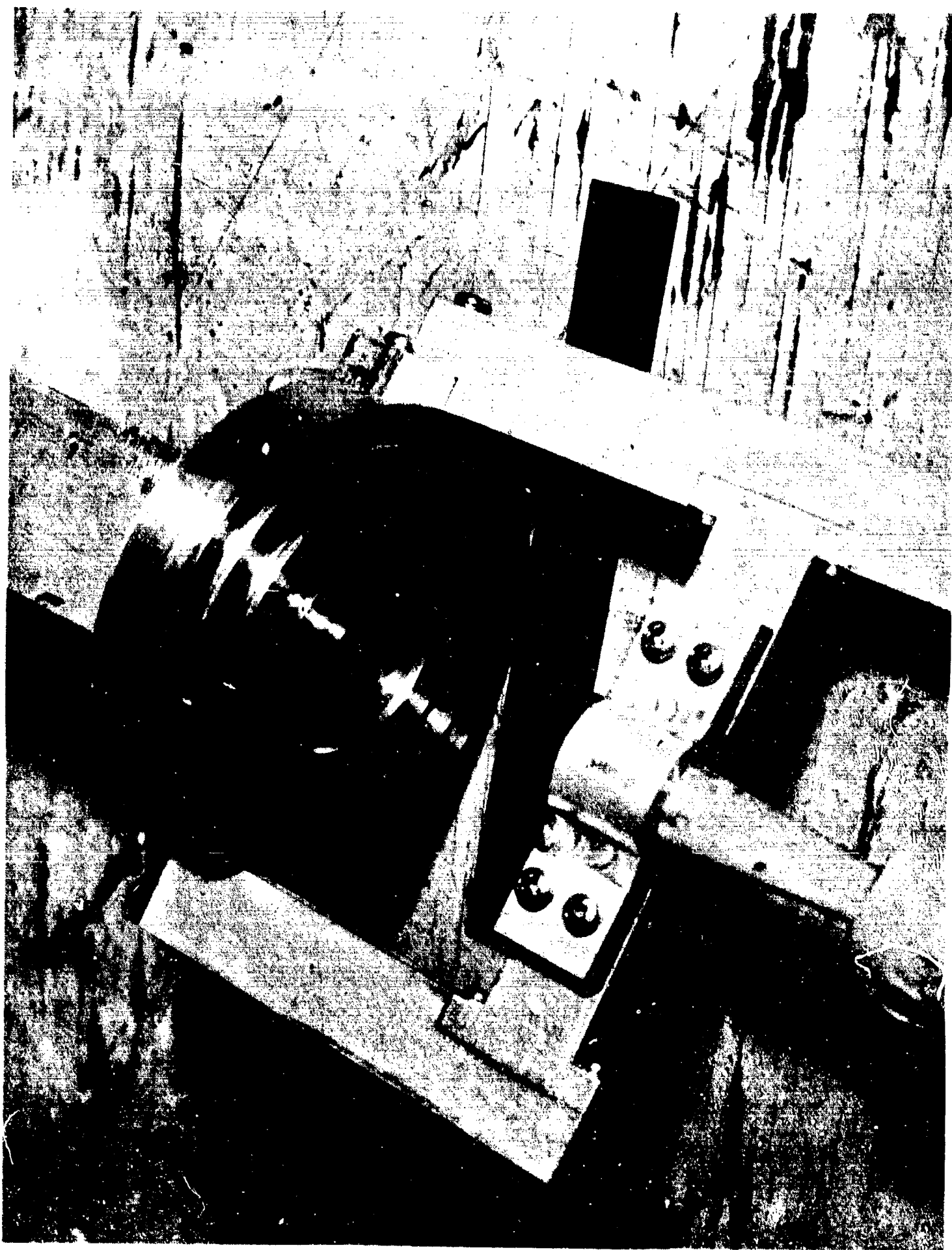


Figure 19. Cross Section of Annular Step Mirror

Figure 20. Experimental Annular Step Disc Feed



A representative set of recorded patterns is shown in Figure 21 for the case of feed horn polarization perpendicular to the plane of the horn support. The upper patterns are for the principal polarization for the three conditions of the feed attitude:

- a. Horizontal polarization (E-plane pattern)
- b. 45-degree polarization (45-degree pattern)
- c. Vertical polarization (H-plane pattern)

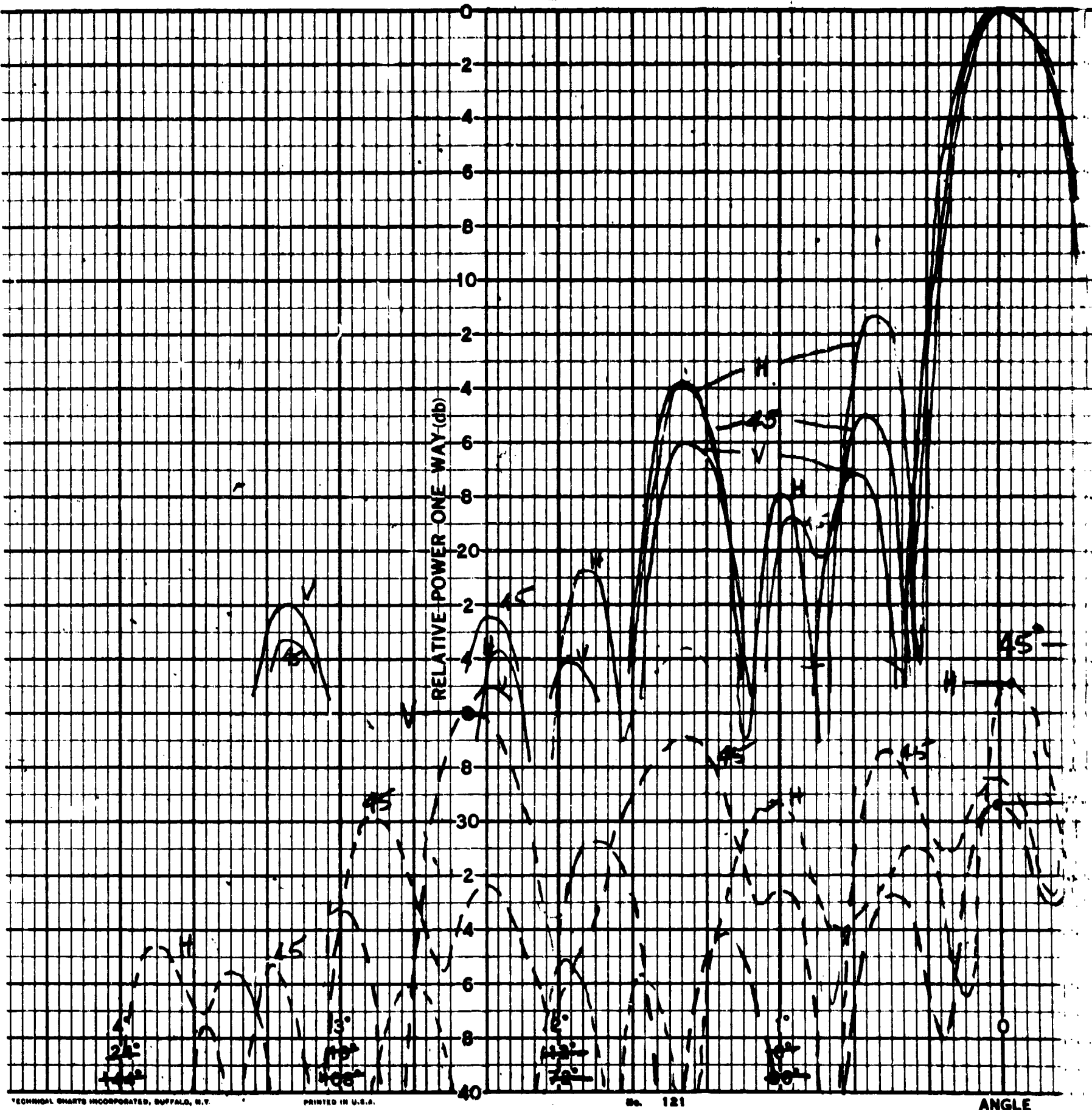
The patterns in the lower portion of the figure are plotted to the same relative scale and show the response for the same feed polarization conditions as a, b and c above but for the source polarization rotated 90 degrees from its attitude in a, b and c, respectively. This is the cross-polarized response of the antenna. The figure presents an overall picture of the patterns showing shape and degree of symmetry. Beamwidths, sidelobe levels, etc., may be read more accurately from following tabulations which include, in some instances, necessary compensating corrections for minor recording system non-linearities.

Figure 22 shows a representative set of patterns recorded for the case of feed horn polarization parallel to the plane of the horn support. These patterns were recorded earlier in the program than those of the previous figure and the lesser degree of symmetry displayed here is attributed to the incomplete recognition, at that time, of the importance of critical adjustment of the masthead angle between the feed axis and the radius line to the axis of rotation. It was subsequently determined that the decibel difference in level between right and left sidelobes is changed at the rate of about 2.1 db per degree as this angle is changed over a small range. It is possible that the cross-polarization level is similarly sensitive to this angle.

The two previous figures were for the feed set close to its design position at $r_p = 0.563$. Figures 23 through 26 summarize the results of pattern changes as the feed position is varied. The abrupt rise of one of the 10-db beamwidth curves to the right of $r_p = 0.565$ is caused by the inclusion of a first sidelobe or shoulder at the 10-db level.

In general, it may be noted in Tables 1 and 2 that at and near the design value for r_p the maximum sidelobe level is about 2 db lower for the perpendicular polarization condition than it is for parallel polarization for a corresponding attitude of the plane of the horn support. In general, the maximum sidelobe level for H-plane patterns is lower (by a maximum amount of 2 db) than for the corresponding E-plane patterns. Also, in general, the sidelobe level is about 4 to 5 db lower for horn support in the plane of the pattern than it is for the horn support perpendicular to the plane of support. Therefore, the dominant cause of difference in sidelobes may be attributed to the attitude of the horn support structure with respect to the plane of the pattern and with respect to the plane of polarization. This conclusion is

BLANK PAGE



A

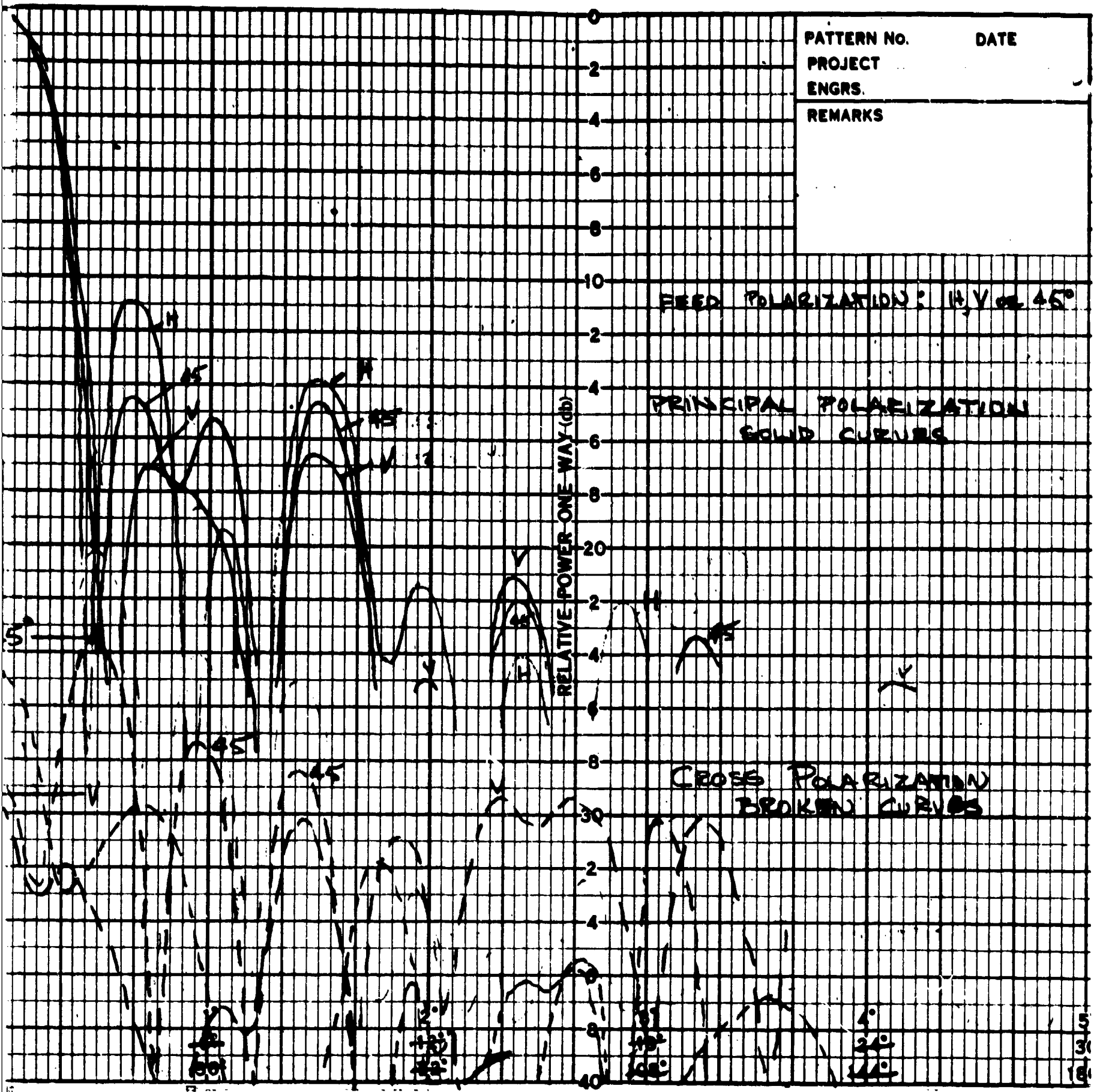
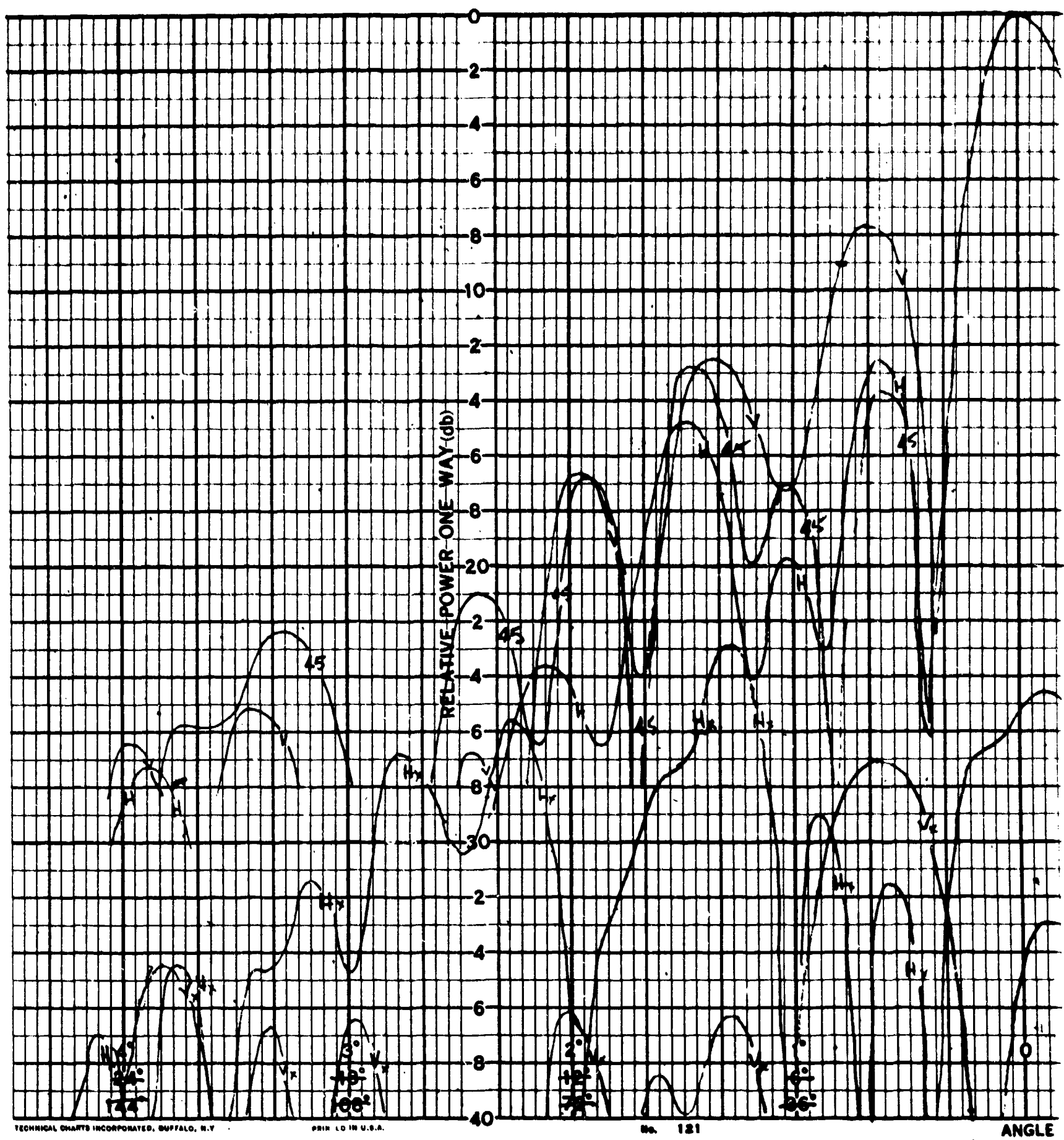


Figure 21. Patterns of ASDF,
Polarization Perpendicular to
Horn Support

B



A

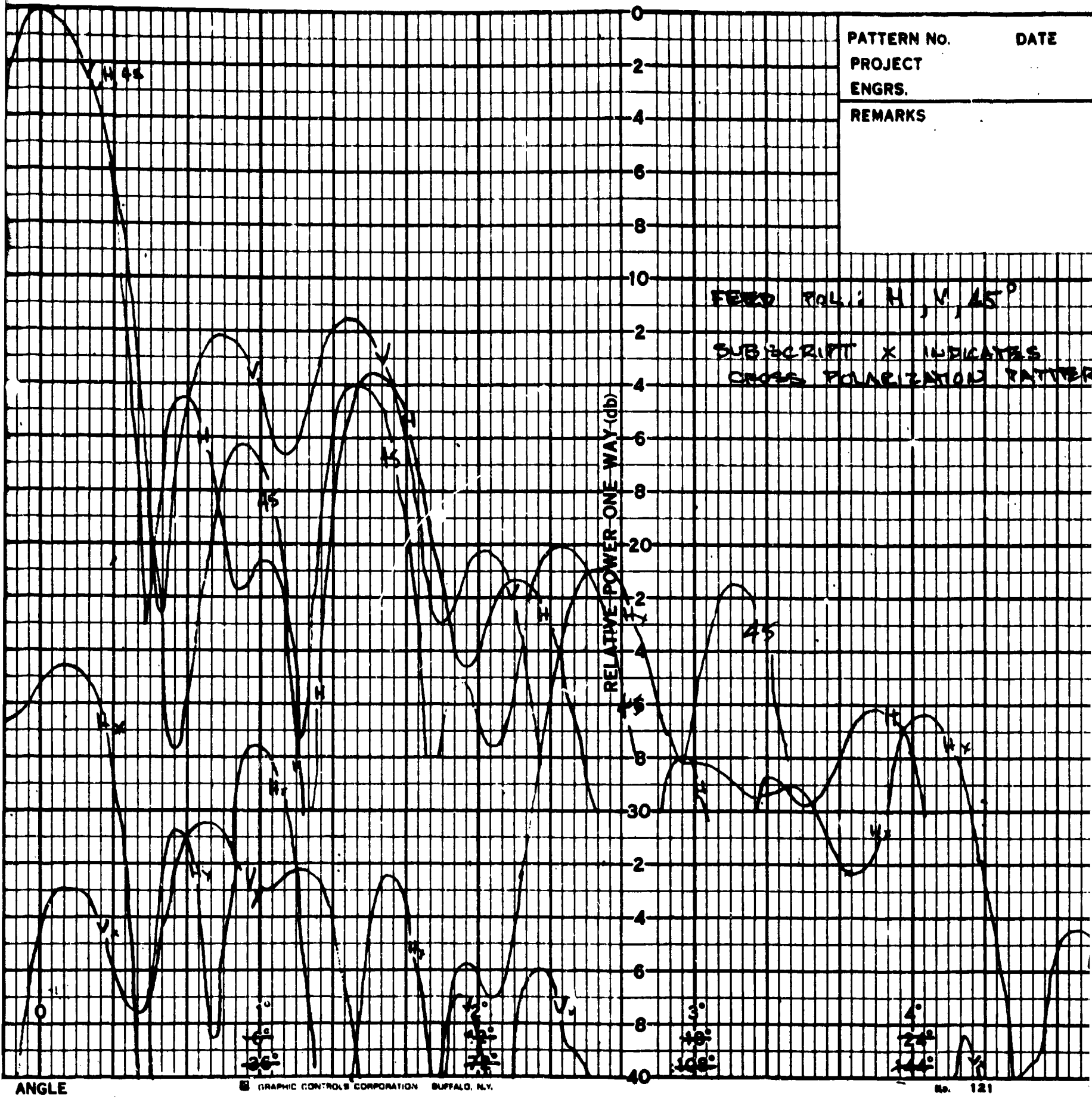


Figure 22. Patterns of ASDF,
Polarization in Plane of Horn
Support

B



Figure 23. Beamwidth as Function of Feed Position, Perpendicular Polarization

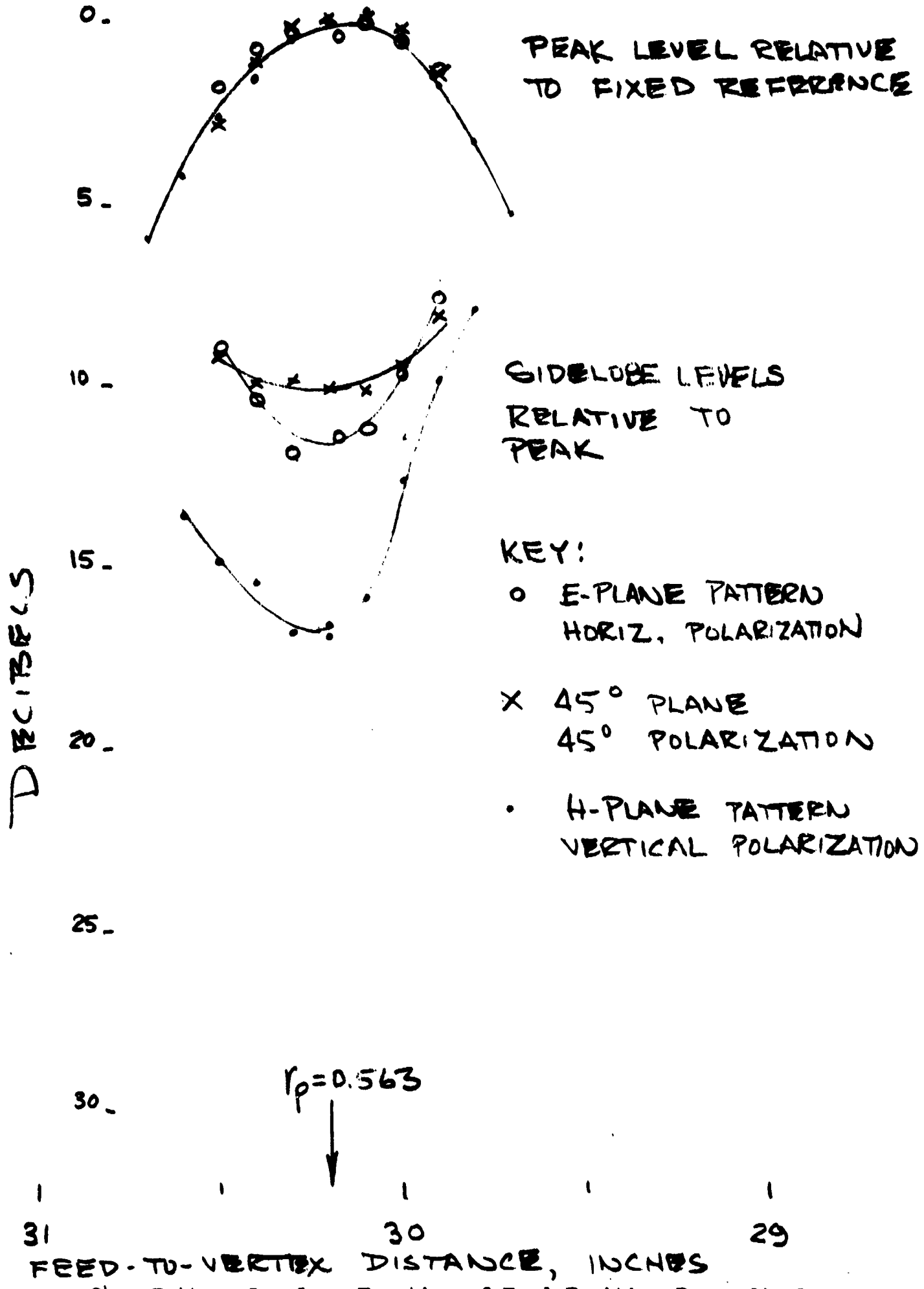


Figure 24. Pattern Level as Function of Feed Position Perpendicular Polarization

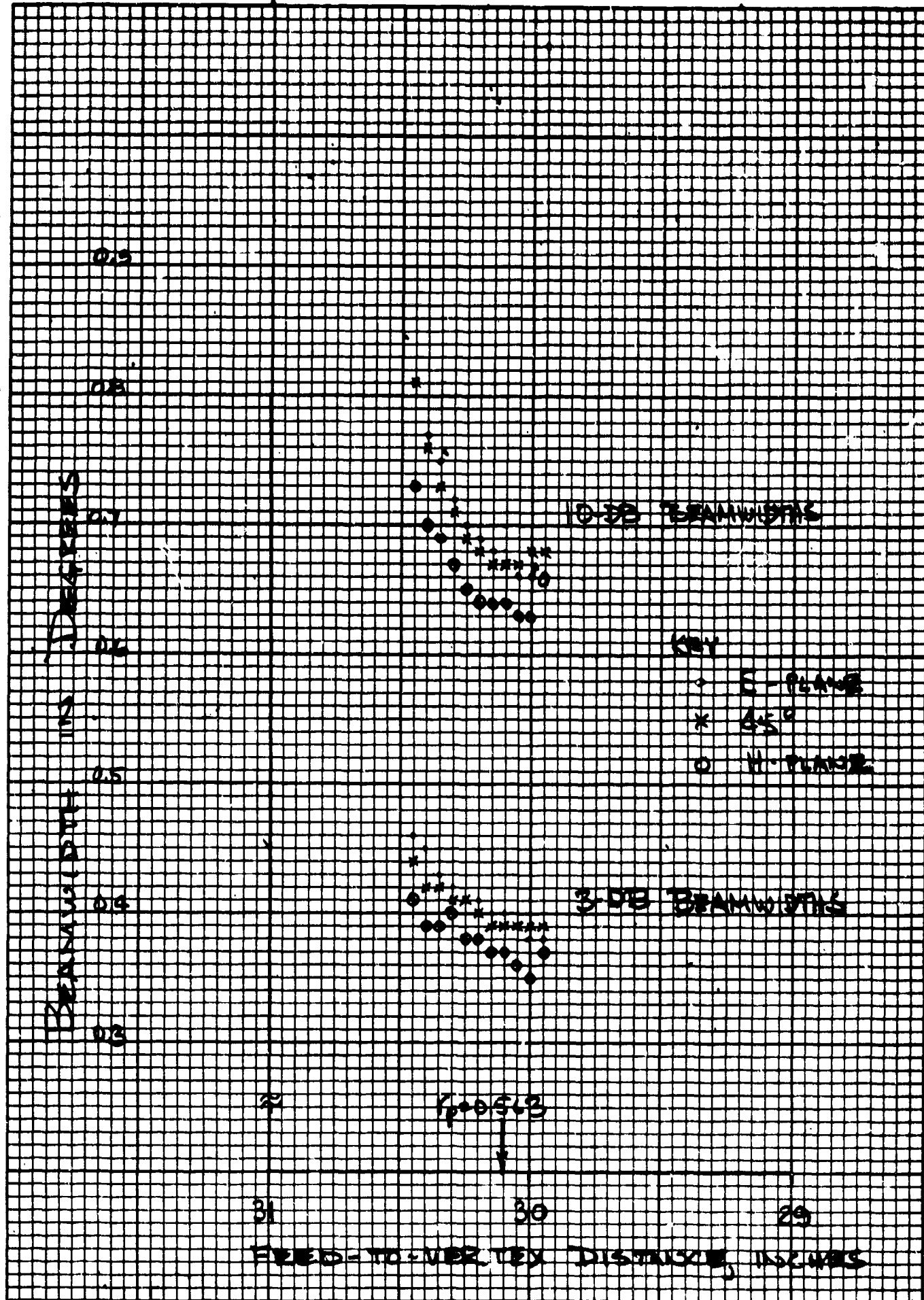


Figure 25. Beamwidth as Function of Feed Position, Parallel Polarization

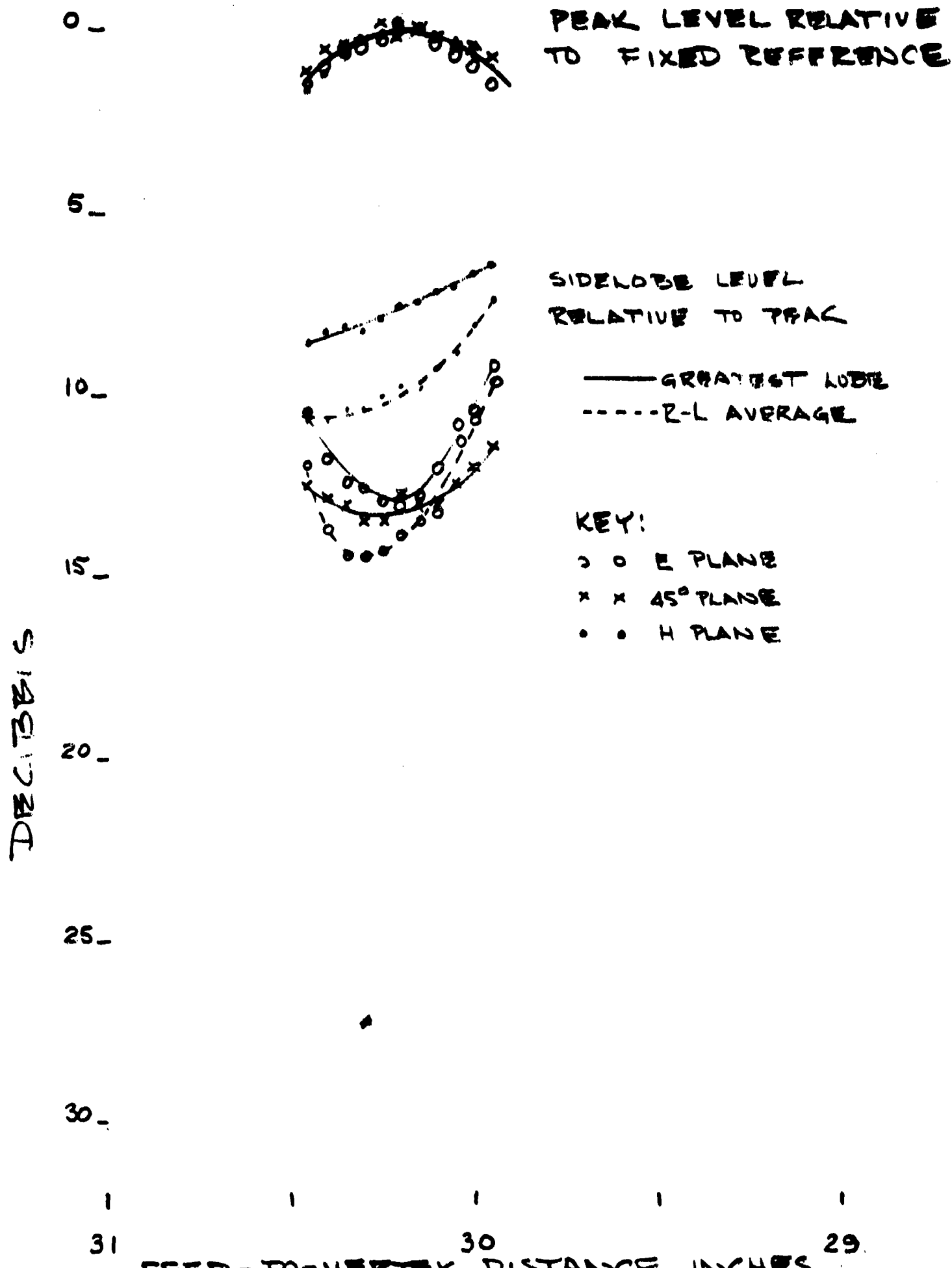


Figure 26. Pattern Level as Function of Feed Position, Parallel Polarization

TABLE 1

SUMMARY OF PATTERN CHARACTERISTICS OF
ANNULAR STEP DISC FEED

LINE	POLAR. REL. TO HORN SUPPORT	DIAGRAM ¹	POLAR.	PLANE OF PATTERN REL. TO			FULL BEAMWIDTHS, DEG.			LEVELS, DB BELOW PEAK FIRST 1.5°		
				FEED	HORN SUPPORT (deg.)	3-DB	10-DB	20-DB	MIL.;	SIDE- LOBE	SIDE- LOBE	GREATEST SIDELOBE
a	PERP.	↑	PRINC.	E	90	0.39	0.62	0.75	0.82	11.0	13.6	11.5
b	PERP.	→	PRINC.	45°	45	0.40	0.67	0.85	0.90	14.2	13.8	13.0
c	PERP.	↓	PRINC.	H	0	0.41	0.70	0.91	1.02	17.2	15.8	16.5
d	PERP.	↔	CROSS	E	90							25.0
e	PERP.	↔	CROSS	45°	45							23.5
f	PERP.	↔	CROSS	H	0							25.8
g	PARA.	↑	PRINC.	E	0	0.35	0.68	0.82	0.89	12.3	13.2	14.0
h	PARA.	↑	PRINC.	45°	45	0.40	0.68	0.88	1.03	13.6	12.8	13.5
i	PARA.	↔	PRINC.	H	90	0.41	0.69	0.85	0.92	7.6	11.3	10.0
j	PARA.	↑	CROSS	E	0							9.9
k	PARA.	↔	CROSS	45°	45							22.8
l	PARA.	↓	CROSS	H	90							26.4

¹ARROW → REPRESENTS POLARIZATION; BROKEN LINE ↓ PLANE OF HORN SUPPORT AS VIEWED FROM VERTEX OF SPHERE LOOKING TOWARD FEED AND SOURCE. PLANE OF PATTERN IS HORIZONTAL IN ALL CASES.

TABLE 2

PATTERN CHARACTERISTICS AVERAGED BY CATEGORY

PATTERN CATEGORY	AVERAGED PATTERNS (LINES, TABLE 1)	FULL BEAMWIDTHS, DEG.			FIRST MISS.	FIRST SIDELOBE	LEVELS, DB BELOW PEAK	GREATEST SIDELOBE
		3-DB	10-DB	20-DB				
PERP. POL. PARA. POL.	a,b,b,c g,h,h,i	0.40 0.40	0.67 0.67	0.84 0.86	0.91 0.97	14.2 (12.4)	14.3 12.5	13.6 11.4 (12.0) ¹
E-PLANE 45°-PLANE H-PLANE	a,g b,h c,i	0.39 0.40 0.41	0.63 0.68 0.70	0.79 0.87 0.88	0.86 0.97	11.7 13.9 (13.6)	13.4 13.3 13.6	11.7 13.3 11.7 (12.9)
	c,g b,h a,i							
0° 45° 90°		0.40 0.40 0.40	0.67 0.68 0.66	0.87 0.87 0.80	0.96 0.87 0.80	14.8 13.9 (10.5)	14.5 13.3 12.5	14.1 13.3 9.3 (10.5)

¹VALUES SHOWN IN PARENTHESIS RESULT FROM AVERAGING RIGHT AND LEFT SIDELOBES IN PATTERN i.

consistent with the known facts that a given optical strip blockage of the horn support should have a greater effect in raising sidelobes when perpendicular to the plane of pattern and a greater effect when parallel to the plane of polarization.

The measured patterns for perpendicular polarization in the H-plane are thus closest to the theoretical patterns for an unblocked circular aperture as shown by the comparison in Table 3.

The response of the experimental antenna was measured relative to a standard-gain pyramidal horn antenna placed immediately before the aperture of the spherical antenna. The pyramidal horn has a gain of 24.7 db. A uniformly illuminated circular aperture of 140-wavelength diameter (the design aperture) has a gain of 52.9 db.

The response of the antenna for the design condition based on the average of ten independent measurements for polarization perpendicular to the plane of the horn support is 4 decibels below that of the uniform aperture. The response for polarization parallel to the plane of the horn support is 6 decibels below that of the uniform aperture based on six independent measurements. These figures are subject to a possible error estimated to be about ± 1 db due to limitations of the test set-up.

The -4 and -6 db values represent the overall antenna efficiency values for the two cases of interest. It is possible to account for -2 db of the total in each case by accumulating the estimated effects of primary spillover (-1.2 db), blockage (-0.7 db) and reflector surface roughness (-0.1 db). The primary spillover was discussed in Section 4.2. The blockage figure is based on the loss of illuminated area due to optical shadowing (a) of 47 square inches of the spherical reflector by the feed horn and by the mounting clamp of the feed horn support and (b) of 224 square inches of the main aperture by the feed support mast and by the three struts which are visible in Figure 8. In 1960 the surface of the reflector was reported in Reference 6 to be within ± 0.014 inch of a true spherical surface. After allowance for effects on the surface of handling and aging the root-mean-square surface deviation is estimated to be 0.007 inch which corresponds to a surface roughness loss of 0.1 db.

TABLE 3

COMPARISON TO THEORETICAL PATTERN OF 140-MILE LENGTH
DIAMETER UNIFORM CIRCULAR APERTURE

PATTERN	FULL BROADBANDS, DEC.			LEWIS, NO REGION MAX		
	3-18	10-18	20-18	FIRST MIN.	SIMILAR STUDIES	CREATOR SIMILAR
c	0.41	0.70	0.91	1.02	17.2	15.8
THEORY	0.42	0.72	0.89	1.00	17.6	23.8

SECTION 5

CONCLUSIONS

The studies on geometric optics have yielded needed insight concerning the focal region of the spherical reflector. The concepts developed lead to simple expressions for many useful relationships in the analysis and synthesis of spherical antennas. The geometric optics approach by itself is incapable of completely describing the focal region effects. The next step includes application of physical optics and the more nearly complete accounting for diffraction effects but is based on the results of the geometric optics. This step, using the method of stationary phase for asymptotic evaluation of the integral expression for fields due to reflector currents, resulted in the numerical evaluation of focal region fields in amplitude and phase for three orthogonal components of polarization. Accuracy of the first order only is attributed to this specific technique because only the initial terms in two Taylor series expansions were retained. Useful plots for focal regions between the caustics were obtained for a number of sets of conditions.

One set of conditions was experimentally duplicated using a 10-ft. spherical reflector at 24 Gc. Movable electric and magnetic dipole-like probes were used to determine the amplitude character of the focal region fields.

The degree of agreement between the calculated amplitude and the measured amplitude distributions is good. Within that region not closer than about 0.5 degree to a caustic the calculated and measured curves are remarkably similar with respect to the level, shape, beamwidth and location of the multiple lobes that typically make up the distribution. Low-level field portions and nulls, are less in agreement than are the lobes. However, the difference often is evidenced more as an asymmetry in the experimental data than as a basic or characteristic difference between theory and experiment.

The validity and effectiveness of both the theoretical and the experimental techniques used to determine focal region fields have been established by the high degree of similitude exhibited by the calculated and measured amplitude distributions for the principal polarization component. The shape of the amplitude distribution is the result of vector summation of multiple (in general, three) contributions each varying in amplitude and phase with respect to the field point position coordinates. It follows that the correct shape can be calculated only provided that the contributions are correct in both phase and amplitude at least in relative sense with respect to one another. Now since these contributions are often varying rapidly in both absolute and relative phase because of the multiple wavelength path-lengths it appears quite improbable for the calculated relative phases are in error. Thus the calculated focal region field phase distributions are indirectly confirmed by the experimental amplitude measurements. The proper performance

of the annular step disc feed, the design of which is critically dependent upon the calculated phase distribution, furnishes additional verification of the calculated phases.

The annular step disc feed is a new form of correcting feed having a simplicity of construction that makes it attractive for the first experimental model work. The annularly stepped zones on the face of the feed mirror are designed to pre-distort the spherical wave from the little feed horn so as to establish a corrected reflected wave progressing toward the spherical reflector. The correction is primarily a phase correction based on the calculated knowledge of the focal region field for an incoming uniform plane wave; only a rough control of amplitude distribution is accomplished by proportioning of the feed horn and the stepped mirror.

The annular step disc feed was built to find out if it is possible to correct for spherical aberration in a transverse feed so as to feed a wide angle of the sphere effectively. The results of tests show that this can be done. The feed is designed to excite a spherical cap having a diameter equal to the radius of curvature, 140 wavelengths. With the corrected feed the reflector has a secondary radiation pattern similar to that of a 140-wavelength diameter uniformly illuminated aperture. Noted differences are small in the main lobe. Experimental sidelobe levels are higher than those predicted by theory. This is attributed partly to the blockage effect of the feed horn support structure and partly to the incomplete amplitude control inherent in the feed design.

Measured overall antenna efficiency (relative to a 1-0-wavelength diameter uniformly excited aperture) of -4 db is obtained with about -2 db accountable to estimated effects of feed horn spillover, blockage and spherical reflector surface roughness. Thus, the remaining -2 db is a measure of the effectiveness of the basic design concept.

Although the feed was deliberately designed to match the focal region field in principal polarization component only, the response of the feed includes an unexpectedly small cross polarization component. (Much of the measured cross polarization energy is attributed to lack of perfection in the experimental setup.) It appeared possible to substitute a dually polarized feed horn for the simple one actually used and thus to obtain readily a dually polarized antenna system. More importantly, however, the polarization performance of the feed led to the re-examination of the whole role played by polarization and a new understanding of its control.

It has been pointed out that the variation of the focal region field with respect to ϕ_p is related to the attitude of the sampling dipole. The electric dipole was used as a basis for all theoretical calculations while the equivalent of a magnetic dipole was used in the experimental work. Nevertheless, excellent agreement was obtained between experiment and theory by accounting for the difference in kind and in attitude of the sampling dipole.

An electric dipole oriented in the \hat{i} , \hat{j} and \hat{k} directions will respond to those same components of electric field and will have response variation with ϕ_p for an incoming wave of \hat{i} polarization as follows, respectively

$$1 - k \cos 2\phi_p \text{ for } \hat{i},$$

$$\sin 2\phi_p \text{ for } \hat{j}, \text{ and}$$

$$\cos \phi_p \text{ for } \hat{k}.$$

The coefficient k is a function of θ_p , r_p and R/λ .

A magnetic dipole with its axis in the \hat{i} , \hat{j} and \hat{k} directions will respond to those components of magnetic field and will have response variation with ϕ_p for an incoming wave of \hat{i} polarization as follows, respectively

$$-\sin 2\phi_p \text{ for } H\hat{i},$$

$$1 + \cos 2\phi_p \text{ for } H\hat{j}, \text{ and}$$

$$\sin \phi_p \text{ for } H\hat{k}.$$

The principal polarization components of an incoming wave of \hat{i} polarization are $E_{\hat{i}}$ and $H_{\hat{i}}$. Therefore, if an electric dipole along \hat{i} and a magnetic dipole along \hat{j} are coupled to a receiver in such a manner as to produce equal and in-phase responses then the combined principal polarization response will have no variation with respect to ϕ_p as the $\pm k \cos 2\phi_p$ terms will cancel. Furthermore, the response to an incoming wave of \hat{j} polarization will be nil regardless of ϕ_p as the $\pm \sin 2\phi_p$ terms representing response to $E_{\hat{i}}$ and $H_{\hat{i}}$ will cancel. Although $E_{\hat{k}}$ and $H_{\hat{k}}$ components will be present for an incoming wave of \hat{i} or \hat{j} polarization the dipoles produce no response to these components. Therefore, the combination of dipoles has response to but a single incoming polarization and this response is completely independent of variation with ϕ_p .

This particular combination of dipoles is the equivalent of a Huygens source (References 10 and 11). For short dipoles the combination has a rotationally symmetric pattern represented by

$$1 + \cos \theta$$

where θ is the co-latitude angle measured from the axis perpendicular to both dipoles.

It follows that more complex sampling probes consisting of combinations of a co-polarized Huygens-source-like elements may be expected to have the same freedom from cross-polarization response and variation with ϕ . If such elements are indeed used as sampling probes or as elements in a corrected transverse feed the analysis is simplified greatly.

The choice of radiating elements used to make up a Huygens-source combination can be made from a variety of existing radiators including dipoles, loops, slots, curved current elements, curved slots, horns, open waveguides, and, perhaps, others. Such choice is appropriate at a later stage of development when more thorough consideration of operative factors may be made.

It may be noted here that the experimental annular step disc feed is shown to embody characteristics of the Huygens source in a particularly simple feed. One way of viewing this feed is to consider it as consisting of an array of many small elements. Each element is a small increment of area of the disc surface. Each element radiates an increment of area of a plane wave in reflecting (or transmitting) the wave originating at the primary feed radiator. The element radiates a plane wave, or one that is nearly so, because the element itself is plane and it is in the far field of the primary feed radiator. The plane wave, having equal strength E and H components, is equivalent to the desired Huygens source. This view breaks down, of course, at the step discontinuities where it does not properly take diffraction effects into account. The validity of the view is partially established by the low level of cross polarization exhibited by the feed.

The simplification of the focal region distribution to a rotationally symmetric single component by use of the polarization viewpoint given above is considered to be an important step.

A second important step is the discovery of the mathematical tool for transforming the computationally available focal region distribution for uniform amplitude aperture distribution into new focal region distributions producing a wide and useful variety of non-uniform aperture distributions. Thus it appears possible to produce rotationally symmetric aperture distributions for low sidelobe requirements and odd symmetry distributions for simultaneous or sequential lobing applications.

This work forms a basis for future developments including control of secondary beam characteristics by control of array type transverse focal region feeds.

REFERENCES

1. Roy C. Spencer and Geoffrey Hyde, "Transverse Focal Region of a Spherical Reflector, Part 1: Geometric Optics", Radio Corporation of America, March 1964, AFCRL-64-992, AD 603788.
2. Geoffrey Hyde and Roy C. Spencer, "Transverse Focal Region of a Spherical Reflector, Part 2: Polarization", Radio Corporation of America, May 1964, AFCRL-64-292II, AD 607477.
3. Geoffrey Hyde, "Transverse Antenna Feeds Focal Region Fields of a Spherical Reflector", Radio Corporation of America, January 1966, AFCRL-66-48.
4. R. C. Spencer, "Fourier Integral Methods of Pattern Analysis", Radiation Laboratory Report 762-1, January 1946.
5. P. Jacquinot and B. Roizen-Dossier, "Apodization", Progress in Optics, Vol. III, E. Wolf, Ed., John Wiley and Sons, Inc., New York, 1964.
6. John Ruze, "Circular Aperture Synthesis", IEEE Trans. on Antennas and Propagation, Vol. AP-12, No. 6, November 1964, pp. 691-694.
7. C. J. Sletten, P. Blacksmith, Jr., F. S. Holt and J. E. Holland, "Line Source Antenna Arrays for Control of Pattern, Dispersion, and Phase", Air Force Cambridge Research Laboratories, June 1963, AFCRL-63-182.
8. Wiley Electronics Co. WER-93, "Final Report on Research Directed Toward Theoretical and Experimental Investigation of Corrected Line Source Feeds", Contract No. AF 19(604)-5718, February 1960, AFCRC-TR-60-122.
9. H. Jasik, "Antenna Engineering Handbook", McGraw-Hill Book Company, Inc., New York, 1961, Chapter 14.
10. E.M.T. Jones, "Paraboloid Reflector and Hyperboloid Lens Antenna", Transactions of IRE, Vol. AP-2, No. 3, July 1954, pp. 119-127.
11. Jerome D. Hanfling, "Mapping of the Far Field Polarization of Antennas by the Stereographic Projection", Thesis for degree M. of E.E., Polytechnic Institute of Brooklyn, June 1960, AD245496.
12. S. Silver, "Microwave Antenna Theory and Design", Vol. 12, Radiation Laboratory Series, McGraw-Hill Book Co., Inc., 1949.
13. E. Jahnke and F. Emde, "Tables of Functions", Dover Publications, 1945.

CONTRIBUTIONS AND ACKNOWLEDGEMENTS

Scientists and engineers who contributed to the work reported are:

D. F. Bowman
J. H. Brumbaugh
G. Hyde
W. Moule
Dr. R. C. Spencer
B. Watson
Dr. F. M. Weiss

Acknowledgement is due also to Dr. A. Boivin, consultant, and to H. Cox, programmer, for their contributions.

Grateful acknowledgement is expressed for helpful discussions with C. J. Sletten, Dr. E. Altschuler, Dr. A. Schnell and others at AFCRL, but especially for those with O. Kerr, Jr.

APPENDIX A

CIRCULAR APERTURE WITH $J_0(vr)$ TAPER

COMPUTATIONS

DEFENSE ELECTRONIC PRODUCTS
MOORESTOWN, NEW JERSEY

S.O. NO. 997285 PAGE 1

ENGR. DFB CHKD

DATE 6.50226 REV. 660217

SUBJECT: CIRCULAR APERTURE WITH $J_0(vr)$ TAPER
ITEM: DERIVATION OF PATTERN EXPRESSION, GAIN

REF. 12

FOLLOWING SILVER¹ (PARA. 6.8) THE PATTERN
OF CIRCULAR APERTURE IS

$$g(\theta, \phi) = \iint_0^{2\pi/a} F(r, \phi') e^{jka \sin \theta \cos(\phi - \phi')} r dr d\phi'$$

WHERE a IS THE RADIUS OF THE APERTURE.
INTRODUCING VARIABLES

$$r = \rho/a; \quad u = \frac{2\pi a}{\lambda} \sin \theta = \frac{\pi D}{\lambda} \sin \theta,$$

THE CORRESPONDING PATTERN FUNCTION IS THEN

$$g(u, \phi) = a^2 \iint_0^{2\pi} f(r, \phi) e^{jur \cos(\phi - \phi')} r dr d\phi.$$

IN OUR CASE $f(r, \phi) = J_0(vr)$ SO

$$\begin{aligned} g(u, \phi) &= a^2 \iint_0^{2\pi} J_0(vr) e^{jur \cos(\phi - \phi')} r dr d\phi \\ &= 2\pi a^2 \int_0^{2\pi} J_0(vr) J_0(ur) r dr. \end{aligned}$$

USING JAHNKE AND EMDE² (P. 146) WE FIND

$$g(u, \phi) = 2\pi a^2 \left[\frac{ur J_0(vr) J_{-1}(ur) - vr J_{-1}(vr) J_0(ur)}{v^2 - u^2} \right]_{r=0}^1$$

$$= 2\pi a^2 \frac{u J_0(v) J_{-1}(u) - v J_{-1}(v) J_0(u)}{v^2 - u^2}$$

$$= 2\pi a^2 \frac{v J_1(v) J_0(u) - u J_0(v) J_1(u)}{v^2 - u^2}$$

COMPUTATIONS

DEFENSE ELECTRONIC PRODUCTS
MOORESTOWN, NEW JERSEY

S.O. No. 997285 PAGE 2

ENGR DFB

CHKD

DATE 650226

REV. 660217

RCA

SUBJECT: CIRCULAR APERTURE WITH $J_0(vr)$ TAPER
ITEM: DERIVATION OF PATTERN EXPRESSIONS, GAIN

THE PEAK VALUE, AT $u=0$, IS

$$g(0, v) = 2\pi a^2 \frac{J_1(v)}{v} = \pi a^2 \Lambda_1(v)$$

THE PATTERN NORMALIZED TO THE PEAK VALUE IS

$$\frac{g(u, \phi)}{g(0, \phi)} = 2 \frac{v J_1(v) J_0(u) - u J_0(v) J_1(u)}{(v^2 - u^2) \Lambda_1(v)}, u \neq v \quad (1a)$$

$$= \frac{J_0^2(u) + J_1^2(u)}{\Lambda_1(u)}, u = v \quad (1b)$$

THE MAXIMUM VALUE OF THE GAIN FUNCTION IS

$$G_M = \frac{4\pi \left| \int_0^a f(r) 2\pi r dr \right|^2}{\lambda^2 \int_0^a |f(r)|^2 2\pi r dr}, \text{ IN GENERAL.}$$

FOR $f(r) = J_0(vr)$

$$G_M = \frac{4\pi \left| \int_0^a J_0(vr) 2\pi r dr \right|^2}{\lambda^2 \int_0^a |J_0(vr)|^2 2\pi r dr}$$

$$= \frac{4\pi |\pi a^2 \Lambda_1(v)|^2}{\lambda^2 \pi a^2 \{ [J_0(v)]^2 + [J_1(v)]^2 \}}$$

$$= \frac{4\pi^2 a^2}{\lambda^2} \frac{\Lambda_1(v)}{J_0^2(v) + J_1^2(v)}$$

61

(2.)

COMPUTATIONS

DEFENSE ELECTRONIC PRODUCTS
MOORESTOWN, NEW JERSEY

S.O. No. 997285

PAGE

3

ENGR. DEB

CHKD

DATE 650226

REV.

660217

SUBJECT: CIRCULAR APERTURE WITH $J_0(v)$ TAPER
ITEM: DERIVATION OF PATTERN EXPRESSION, GAINFOR UNIFORM ILLUMINATION $G_M = G_0$

$$G_0 = \frac{4\pi^2 a^2}{\lambda^2}$$

THE APERTURE DISTRIBUTION EFFICIENCY
IS, THEREFORE

$$\eta_{AD} = \frac{G_M}{G_0} = \frac{J_1(v)}{J_0^2(v) + J_1^2(v)} \quad (3.)$$

THE APERTURE TAPER IN DB IS N WHICH

$$N = 20 \log_{10}(J_0(v))$$

CORRESPONDING VALUES OF N, V AND η_{AD}
ARE TABULATED BELOW

N (DB)	V (RADIAN)	η_{AD} (RATIO)
4.9	1.4	.985
9.4	1.8	.92
13.0	2.0	.87
15.6	2.1	.84
19.1	2.2	.80
25.1	2.3	
27.0	2.32	.74
32.6	2.36	
46.0	2.4	.69
	2.5	.64
	2.6	.57

APPENDIX B

A CONCRETE REFLECTOR FOR EXPERIMENTAL WORK

A problem was presented in the procurement of a 10 to 14 ft. spherical metallic surface suitable for use as a microwave reflector in the experimental investigation. The spherical reflector, unlike those of paraboloidal shape, is not available in the form of spinnings or machined castings made with accessible tooling. As a large investment in new tooling is not warranted for a single experimental spherical reflector other approaches were investigated. A practical solution appears to have been found in a preliminary design based on a concrete shell. The spherical surface is generated by a sweep template rotating about the reflector. A better spherical surface is then obtained by applying grout to the concrete. Finally, after a suitable setting time the surface may be trimmed to a still better spherical shape by a grinding attachment fitting the same tooling structure as used for the template. The finished spherical surface is then flame sprayed to produce a uniform metallic coating.

The principal advantage of the concrete technique is the low cost for producing a single reflector having a spherical surface accurate to within $\pm 1/32$ inch or less. It is estimated that a 14-ft. diameter concrete reflector having a radius of curvature of 14 ft. can be produced at a cost of \$7,000, which is at least 50 percent less than for comparable reflectors by other techniques. Moreover, the concrete reflector produces exceptional stability during prolonged testing.

The concrete reflector, at an estimated weight of 14,000 lbs., is three to seven times as heavy as other types. The weight is an acceptable disadvantage during the initial handling and mounting in the experimental set up. The weight imposes no additional penalty as the reflector mount is already required to be highly rigid, and hence strong, in order to maintain low deflections under wind and other variable loads.

The concrete reflector was not used in this program as a suitable aluminum one was made available by Air Force Cambridge Research Laboratories. However, this technique of construction appears to have merit for spherical (or other rotationally symmetric) shapes.

UNCLASSIFIED

Security Classification

DOCUMENT CONTROL DATA - R&D

(Security classification of title, body of abstract and indexing annotation must be entered when the overall report is classified)

1. ORIGINATING ACTIVITY (Corporate author) Radio Corporation of America Missile and Surface Radar Division Moorestown, New Jersey	2a. REPORT SECURITY CLASSIFICATION UNCLASSIFIED
2b. GROUP	

2. REPORT TITLE

TRANSVERSE ANTENNA FEEDS

4. DESCRIPTIVE NOTES (Type of report and inclusive dates)

Final report Scientific Period covered: January 1963-December 1965

5. AUTHOR(S) (Last name, first name, initial)

BOWMAN, DAVID F.

6. REPORT DATE January 1966	7a. TOTAL NO. OF PAGES 63	7b. NO. OF REFS 13
8a. CONTRACT OR GRANT NO. AF 19(628)-2758	8a. ORIGINATOR'S REPORT NUMBER(S)	
8b. PROJECT AND TASK NO. 4600-07		
c. DOD ELEMENT 62405304	8d. OTHER REPORT NO(S) (Any other numbers that may be assigned this report) AFCRL-66-49	
d. DOD SUBELEMENT 674600		

10. AVAILABILITY/LIMITATION NOTICES

DISTRIBUTION OF THIS DOCUMENT IS UNLIMITED

11. SUPPLEMENTARY NOTES	12. SPONSORING MILITARY ACTIVITY HQ. AFCRL, OAR (CRD) United States Air Force L.G.Hanscom Field, Bedford, Mass.
-------------------------	---

13. ABSTRACT

This study of the transverse focal region of a spherical reflector includes theoretical analyses centered on geometric optics, on vector polarization and on diffraction integrals of physical optics and their evaluation by the method of stationary phase. The results of the numerical evaluation of the focal region field for an incoming wave of uniform amplitude and phase agree with experimental measurements taken on a 10-ft. spherical reflector operating at 24 Gc. An annular step disc feed was designed using the calculated field as a basis. This transverse feed is designed to correct for spherical aberration over an included angle of the sphere of 120 degrees. The measured secondary patterns show agreement with the theory in the region of the main lobe. The disagreement in the area of the side lobes is attributed partly to blockage introduced by the feed horn support and partly to incomplete control of illumination amplitude. Methods are described for minimizing complexity due to polarization and for determining feed distributions required for non-uniform amplitude aperture distributions.

DD FORM 1 JAN 64 1473

UNCLASSIFIED

Security Classification

UNCLASSIFIED

Security Classification

14. KEY WORDS	LINK A		LINK B		LINK C	
	ROLE	WT	ROLE	WT	ROLE	WT
Antenna Spherical Reflector Scanning Antenna Transverse Focal Region Antenna Feed Spherical Aberration Correcting Feed Annular Step Disc Feed Polarization Control Aperture Illumination Control						
INSTRUCTIONS						
1. ORIGINATING ACTIVITY: Enter the name and address of the contractor, subcontractor, grantees, Department of Defense activity or other organization (<i>corporate author</i>) issuing the report.	10. AVAILABILITY/LIMITATION NOTICES: Enter any limitations on further dissemination of the report, other than those imposed by security classification, using standard statements such as:					
2a. REPORT SECURITY CLASSIFICATION: Enter the overall security classification of the report. Indicate whether "Restricted Data" is included. Marking is to be in accordance with appropriate security regulations.	(1) "Qualified requesters may obtain copies of this report from DDC." (2) "Foreign announcement and dissemination of this report by DDC is not authorized." (3) "U. S. Government agencies may obtain copies of this report directly from DDC. Other qualified DDC users shall request through ." (4) "U. S. military agencies may obtain copies of this report directly from DDC. Other qualified users shall request through ." (5) "All distribution of this report is controlled. Qualified DDC users shall request through ."					
2b. GROUP: Automatic downgrading is specified in DoD Directive 5200.10 and Armed Forces Industrial Manual. Enter the group number. Also, when applicable, show that optional markings have been used for Group 3 and Group 4 as authorized.						
3. REPORT TITLE: Enter the complete report title in all capital letters. Titles in all cases should be unclassified. If a meaningful title cannot be selected without classification, show title classification in all capitals in parenthesis immediately following the title.						
4. DESCRIPTIVE NOTES: If appropriate, enter the type of report, e.g., interim, progress, summary, annual, or final. Give the inclusive dates when a specific reporting period is covered.						
5. AUTHOR(S): Enter the name(s) of author(s) as shown on or in the report. Enter last name, first name, middle initial. If military, show rank and branch of service. The name of the principal author is an absolute minimum requirement.						
6. REPORT DATE: Enter the date of the report as day, month, year, or month, year. If more than one date appears on the report, use date of publication.						
7a. TOTAL NUMBER OF PAGES: The total page count should follow normal pagination procedures, i.e., enter the number of pages containing information.						
7b. NUMBER OF REFERENCES: Enter the total number of references cited in the report.						
8a. CONTRACT OR GRANT NUMBER: If appropriate, enter the applicable number of the contract or grant under which the report was written.						
8b, 8c, & 8d. PROJECT NUMBER: Enter the appropriate military department identification, such as project number, subproject number, system numbers, task number, etc.						
9a. ORIGINATOR'S REPORT NUMBER(S): Enter the official report number by which the document will be identified and controlled by the originating activity. This number must be unique to this report.						
9b. OTHER REPORT NUMBER(S): If the report has been assigned any other report numbers (either by the originator or by the sponsor), also enter this number(s).						
If the report has been furnished to the Office of Technical Services, Department of Commerce, for sale to the public, indicate this fact and enter the price, if known.						
11. SUPPLEMENTARY NOTES: Use for additional explanatory notes.						
12. SPONSORING MILITARY ACTIVITY: Enter the name of the departmental project office or laboratory sponsoring (paying for) the research and development. Include address.						
13. ABSTRACT: Enter an abstract giving a brief and factual summary of the document indicative of the report, even though it may also appear elsewhere in the body of the technical report. If additional space is required, a continuation sheet shall be attached.						
It is highly desirable that the abstract of classified reports be unclassified. Each paragraph of the abstract shall end with an indication of the military security classification of the information in the paragraph, represented as (TS), (S), (C), or (U).						
There is no limitation on the length of the abstract. However, the suggested length is from 150 to 225 words.						
14. KEY WORDS: Key words are technically meaningful terms or short phrases that characterize a report and may be used as index entries for cataloging the report. Key words must be selected so that no security classification is required. Identifiers, such as equipment model designation, trade name, military project code name, geographic location, may be used as key words but will be followed by an indication of technical context. The assignment of links, rules, and weights is optional.						

UNCLASSIFIED

Security Classification